

Library Copy
A. 212125 R01

Copy 43
RM SL53G10

~~CONFIDENTIAL~~

~~UNCLASSIFIED~~

NACA

CLASSIFICATION CHANGE

Unclassified Required
Report No. *13958* *PL 4-17-75*
Date *3/98*

RESEARCH MEMORANDUM

for the

U. S. Air Force

LOW-SPEED INVESTIGATION OF THE STATIC LATERAL STABILITY
AND CONTROL CHARACTERISTICS OF A 1/6-SCALE MODEL
OF THE REPUBLIC XF-84H AIRPLANE WITH
THE PROPELLER OPERATING

By William C. Sleeman, Jr., and William D. Morrison, Jr.

Langley Aeronautical Laboratory
Langley Field, Va.

CLASSIFICATION CHANGED **FOR REFERENCE**

UNCLASSIFIED

~~CONFIDENTIAL~~

NOT TO BE TAKEN FROM THIS ROOM

Area Res. abs. Effective
Priority of *FRN-114* Date *4-8-57*
CLASSIFIED DOCUMENT

ND 4-30-57

This material contains information affecting the National Defense of the United States within the meaning of the espionage laws, Title 18, U.S.C., Secs. 793 and 794, the transmission or revelation of which in any manner to an unauthorized person is prohibited by law.

NATIONAL ADVISORY COMMITTEE FOR AERONAUTICS

WASHINGTON

JUN 25 1953

~~CONFIDENTIAL~~

~~UNCLASSIFIED~~



NATIONAL ADVISORY COMMITTEE FOR AERONAUTICS

RESEARCH MEMORANDUM

for the

U. S. Air Force

LOW-SPEED INVESTIGATION OF THE STATIC LATERAL STABILITY
AND CONTROL CHARACTERISTICS OF A 1/6-SCALE MODEL
OF THE REPUBLIC XF-84H AIRPLANE WITH
THE PROPELLER OPERATING

By William C. Sleeman, Jr., and William D. Morrison, Jr.

SUMMARY

An investigation was made to determine the static lateral stability and control characteristics of a 1/6-scale model of the Republic XF-84H airplane with the propeller operating. The model had a 40° swept wing of aspect ratio 3.45 and had a thin 3-blade supersonic-type propeller. Many modifications to the basic configuration were investigated in attempts to alleviate lateral and directional trim problems which appeared to be associated with propeller slipstream rotation. Although significant benefits were realized with several modifications, none of those tested would be expected to afford satisfactory behavior for all normal flight conditions.

A marked left-wing roll-off tendency was indicated at high angles of attack for the basic model configuration. Projection of only the left slat was the most effective remedy found for this problem with the propeller operating. The use of differential wing-flap deflection also appeared to offer a promising means for reducing the roll-off tendency with power on.

The large sidewash over the vertical tail, associated with slipstream rotation, severely restricted the conditions for which directional trim could be maintained. A small triangular dorsal fin, oriented opposite to the slipstream rotation, was found very effective in reducing the adverse sidewash flow at the tail.

~~CONFIDENTIAL~~

INTRODUCTION

At the request of the U. S. Air Force, a series of wind-tunnel tests was conducted in the Langley 300 MPH 7- by 10-foot tunnel of a 1/6-scale model of the Republic XF-84H airplane. The configuration tested had a 40° swept wing of aspect ratio 3.45 and represented a fighter-type airplane driven by a single supersonic propeller. Power-off longitudinal and lateral characteristics of the model are presented in reference 1 and longitudinal stability results with the propeller operating are presented in reference 2. The present investigation was made to determine the power-on lateral stability and control characteristics of the model and to explore means for alleviating any deficiencies encountered.

Because serious lateral and directional trim problems were indicated by data for the basic model, the investigation was extended to study many modifications designed to alleviate these difficulties. Power-on lateral stability characteristics were obtained through the angle-of-attack range with flaps deflected and retracted, and a few tests were made through a range of sideslip angles. Tests were also made of the fuselage alone through a range of sideslip angles with and without the propeller operating.

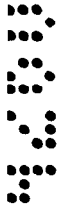
Flow over the wing surface was studied by means of tufts attached to the wing and surveys of the flow behind the model were made by using a tuft grid.

COEFFICIENTS AND SYMBOLS

The data obtained in this investigation are presented as standard NACA coefficients of forces and moments. The system of stability axes employed, together with an indication of the positive forces, moments, and angular displacements are presented in figure 1. Moment coefficients are given about the center-of-gravity location shown in figure 2 (15 percent mean aerodynamic chord, on the thrust line).

The coefficients and symbols are defined as follows:

C_L	lift coefficient, $Lift/qS$
C_X	longitudinal-force coefficient, X/qS
C_Y	lateral-force coefficient, Y/qS
C_l	rolling-moment coefficient, L/qSb



C_m	pitching-moment coefficient, $M/qS\bar{c}$
C_n	yawing-moment coefficient, N/qSb
T_c	effective-thrust disk-loading coefficient, $T_e/\rho V^2 D^2$
Q_c	torque disk-loading coefficient, $Q/\rho V^2 D^3$
V/nD	propeller advance-diameter ratio
η	propulsive efficiency, $T_e V / \rho n Q_c$
X	longitudinal force along X-axis (Drag = $-X$), lb
Y	lateral force along Y-axis, lb
Z	force along Z-axis (Lift = $-Z$), lb
L	rolling moment about X-axis, ft-lb
M	pitching moment about Y-axis, ft-lb
N	yawing moment about Z-axis, ft-lb
T_e	effective propeller thrust, lb
Q	propeller torque, ft-lb
q	free-stream dynamic pressure, $\frac{1}{2}\rho V^2$, lb/sq ft
V	free-stream velocity, ft/sec
ρ	air density, slugs/cu ft
S	wing area, sq ft (9.03 on model, excluding area of inlet ducts)
c	local streamwise chord, ft
\bar{c}	wing mean aerodynamic chord, ft (1.67 on model)
b	wing span, ft (5.59 on model); also propeller blade section chord, ft
D	propeller diameter, ft (2.00 on model)



R	propeller radius, ft
r	radius to any propeller blade element, ft
h	propeller blade section maximum thickness, ft
n	propeller rotational speed, rps
α	angle of attack of thrust line, deg
β	angle of sideslip, deg; also propeller blade angle, deg
i_t	stabilizer incidence relative to thrust line, positive when trailing edge is down, deg
i_f	vertical fin offset angle, positive leading edge to left, deg
i_l	triangular dorsal fin offset angle, positive leading edge to right, deg
δ_r	rudder deflection, positive trailing edge to left, deg
δ_l	deflection of flap on triangular dorsal fin, positive trailing edge to left, deg
δ_f	wing-flap deflection, deg
δ_a	aileron deflection, deg

Subscripts:

β denotes partial derivative of a coefficient with respect to sideslip; for example, $C_{l\beta} = \frac{\partial C_l}{\partial \beta}$

L,R denote deflection of left and right wing flap, respectively

MODEL AND APPARATUS

The basic model used in this investigation was a 1/6-scale model of the Republic XF-84H airplane. The wing had 40° sweepback of the quarter-chord line, aspect ratio 3.45, taper ratio 0.578, and had NACA 64A010 airfoil sections normal to the quarter-chord line. A two-view drawing of the model is presented in figure 2 and a photograph of the model installed

in the Langley 300 MPH 7- by 10-foot tunnel is given as figure 3. Tabulated geometric characteristics of the basic model are given in table I. The model was supplied by Republic Aviation Corporation and was not checked for accuracy.

Differences in the model and proposed airplane configuration are indicated in figure 2 by dashed lines. Inasmuch as no attempt was made to simulate air flow through the model, the inlets and jet exit were faired over as shown. It was not feasible to duplicate the nonrotating propeller spinner nose on the model and a hemispherical spinner nose was used instead. The thrust line of the model coincided with the fuselage center line; whereas the airplane design is to incorporate 1° of downward tilt of the thrust line relative to the fuselage center line.

Geometric characteristics of the solid-steel model propeller are given in figure 4. The blade angle used in all tests was 16.5° at 0.75R and was selected on the basis of simulating the thrust-torque relationship for the airplane at maximum power and high thrust. The propeller was driven by a 47-horsepower electric motor in the model. The rotational speed of the propeller was determined by observation of a stroboscopic frequency indicator which indicated the output frequency of a small alternator on the motor shaft. The accuracy of the frequency indicator was within ±0.05 percent.

Many modifications to the basic model were tested in attempts to alleviate lateral and directional trim difficulties encountered in the course of the investigation. A drawing of the various devices tested, showing their positions on the model, is presented in figure 5.

Flow studies were made in the region of the tail by means of a tuft grid located approximately 1.5 wing semispans behind the center of gravity. The horizontal and vertical tails were replaced by unswept 1/8-inch-diameter rods which indicated the location of the vertical tail, the horizontal tail used in this investigation, and also high and low tail positions.

TESTS AND RESULTS

Test conditions.- Tests were made in the Langley 300 MPH 7- by 10-foot tunnel at dynamic pressures of 4, 6, and 8 pounds per square foot, which corresponded to airspeeds of approximately 40, 48, and 56 miles per hour, respectively. The test Reynolds numbers for these test conditions were approximately 0.64×10^6 , 0.76×10^6 , and 0.90×10^6 based on the wing mean aerodynamic chord of 1.67 feet. The different tunnel speeds used in the tests were selected in order to

obtain maximum thrust coefficients for the simulated power conditions desired.

The propeller calibrations and wing-off tests were made with the model mounted on a single centrally located vertical support strut. All other tests were made with the model supported by its wings through a twin strut system as indicated in figure 3. The presence of the wing support struts prevented the use of the main landing wheels and therefore tests of the flap-deflected configurations (landing and take-off conditions) were made with only the nose wheel extended. The slats and nose wheel were extended, except where indicated, when the flaps were deflected.

Test procedure.- A propeller calibration was made with the propeller on the clean fuselage (wing, canopy, dorsal, empennage, and tail skid removed) mounted on the single support strut and the results are presented in figure 6. The propeller was calibrated by measuring the resultant longitudinal force, minimum motor current, and rolling moment of the model at 0° angle of attack for a range of propeller speeds. Effective propeller thrust was computed from the following relationship:

$$T_e = X_R - X_0$$

where X_R is the resultant longitudinal force obtained with the propeller operating and X_0 is the longitudinal force of the model with the propeller removed.

Torque coefficients presented in figure 6 were obtained from measured rolling moments and these results were in excellent agreement with those determined by use of a calibration of motor torque as a function of minimum motor current.

Some of the power-on tests simulated a constant-power flight condition, which was based on an operating chart obtained at zero sideslip angle. For these tests, the propeller speed and angle of attack of the model were adjusted to correspond to the relationship of T_c and C_L given in figure 7. The power conditions of figure 7 are for a gross weight of 16,000 pounds at sea-level altitude and were selected to simulate the most extreme constant-power flight conditions that might be encountered on this airplane. Power A represents the military power rating of 7,070 horsepower for the XT54-A-2 engine and power B (approach power) is 60 percent of normal power. For tests made at a given value of T_c , the propeller speed was held constant while the angle of sideslip or pitch was varied.

Lateral stability derivatives were obtained from pitch tests at sideslip angles of $\pm 5^\circ$ by assuming a straight-line variation between these points.

Both the horizontal and vertical tails were removed for all the tail-off tests of this investigation.

Corrections.- Jet-boundary corrections to the angles of attack, longitudinal-force coefficients, and tail-on pitching-moment coefficients were obtained from reference 3. The following corrections were added to the data

$$\Delta\alpha = 1.02C_{L_W} \text{ (deg)}$$

$$\Delta C_X = -0.0155C_{L_W}^2$$

$$\Delta C_m = -7.39C_{L_W} \left(\frac{0.220}{\sqrt{\sigma}} - 0.116 \right) \frac{\partial C_m}{\partial i_t}$$

where

$$C_{L_W} = C_L - (\Delta C_L)_{\text{propeller thrust}}$$

$$(\Delta C_L)_{\text{propeller thrust}} = T_c \frac{2D^2}{S} \sin \alpha$$

σ tail lift-effectiveness parameter, $\frac{\partial C_m}{\partial i_t} / -0.022$

Blockage corrections have not been applied to the data.

No systematic evaluation of support tares has been made and corrections for support interference were not applied to the data. Results of a few tare tests, however, have indicated that the wing support tares for pitch tests were small and were associated primarily with a small change in longitudinal trim. Single support tares were evaluated for

the propeller calibrations and were found to be negligible for resultant longitudinal-force coefficients.

Results.- The figures presenting the results are as follows:

	Figure
Typical model characteristics at zero sideslip	8
Modifications to improve lateral trim	9 to 12
Rudder effectiveness, basic model	13
Modifications to improve directional trim	14 and 15
Lateral stability derivatives:	
$\delta_f = 0^\circ$	16
$\delta_f = 40^\circ$, slats extended	17
Aerodynamic characteristics in sideslip:	
Wing off	18
Basic model, $\delta_f = 0^\circ$	19
Basic model, $\delta_f = 40^\circ$, slats extended	20
Effect of triangular dorsal fin, $\delta_f = 40^\circ$, slats extended	21
Wing-surface-tuft photographs	22
Tuft-grid photographs	23

DISCUSSION

Typical effects of propeller operation on the longitudinal and lateral characteristics in pitch are presented in figure 8 to illustrate some of the problems encountered on the basic configuration. The longitudinal instability found at moderate angles of attack and means of alleviating this problem were discussed in references 1 and 2. It is seen in figure 8 that application of power imposes some additional problems of lateral and directional control as indicated by large rolling and yawing moments at high angles of attack with the controls neutral. Most of the discussion of results is concerned with causes for and means of alleviating these control problems.

Lateral Trim at Zero Sideslip

Basic model.- The approximate symmetry of the flow over the wing without power is indicated in the tuft photographs of figure 22(a) and the rolling moment data of figure 8. When power was applied, however, large negative rolling moments were evident at high angles of attack. The dashed curve of figure 8 indicates the maximum rolling moment that could be controlled by the ailerons (obtained from ref. 1) and it is

seen that some means for providing additional lateral control with power on is needed at high angles of attack.

Although it is very difficult to interpret tuft photographs in terms of wing lift, some insight into possible reasons for the roll-off tendency may be found in the photographs of figure 22(b). Photographs of the two wing semispans taken simultaneously show a considerably different flow pattern for the left and right wing surfaces at high angles of attack. Comparison of these photographs with those of figure 22(a) indicates that occurrence of flow separation was accelerated on the side of the up-going propeller blade (left wing) and delayed on the side of the down-going blade. This asymmetry of separation could account for the large rolling moments through a relative loss in lift on the left wing, or by a lateral center of pressure movement to the right on both wings at high angles of attack. The effects of this asymmetric separation add to rolling moments associated with propeller torque to produce the large left roll-off tendency with power on.

Modifications to basic model.- Several devices were studied in an attempt to reduce the rolling moments by reducing slipstream rotation effects on the side of the up-going propeller blade. Figures 9(b) and 10(b) show that some reduction in rolling moment at high angles of attack could be effected by use of a properly located fin ahead of the wing. It was realized that addition of a lifting surface ahead of the center of gravity would adversely affect the longitudinal stability as shown in figures 9(a) and 10(a). It is of interest to note, however, that the smaller triangular fin (fig. 10) gave less adverse longitudinal stability change and retained the rolling-moment benefits of the best square fin arrangement (fig. 9).

Results of other attempts to improve lateral trim characteristics are also presented in figure 10 and none of these modifications afforded significant improvements.

Another approach to the lateral-control problem was the use of asymmetric deflection of wing controls (flaps and slats) to compensate for the aerodynamic asymmetry associated with the rotating propeller slipstream. Results pertaining to the use of slat deflection are presented in figure 11. Deflection of both wing slats did not effect an appreciable reduction in rolling moments for the neutral aileron condition with flaps retracted. It might be expected, however, that some improvements could be attained through increased aileron effectiveness with the slats out. The beneficial effect of the projected slats on the flow over the wing is shown in photographs of wing-surface tufts in figure 22(c). Extension of only the left slat (fig. 11) appeared to be an effective means of alleviating the left roll-off tendency with power on; however, this arrangement would probably not be satisfactory

for all power conditions. Results obtained with the propeller wind-milling and the left slat out, (fig. 11(b)) for example, show that, in the event of power failure, a large right-wing roll-off tendency would occur.

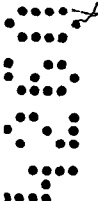
A few tests were made to investigate the use of asymmetric flap deflection and the results are presented in figure 12 as a function of thrust coefficient. Deflection of only the left flap afforded a substantial reduction in rolling moment throughout the thrust range investigated; whereas, deflection of only the right flap showed a marked adverse effect. The use of asymmetric flap deflection shows promise from the standpoint of practical application in that the flaps could be arranged to operate differentially with the existing ailerons or provide differential deflection after full aileron deflection was reached. It should be noted that the results of figure 12 are limited for making an evaluation of differential flap control because the data were obtained at a moderate angle of attack where the rolling moments were not as large as at higher angles. Because the model was not provided with ailerons on both wings, a complete evaluation of lateral control characteristics was not obtained. It appears, however, that additional means of obtaining lateral control must be devised inasmuch as none of the modifications tested eliminated the large change in rolling moment with power at high angles of attack.

Directional Trim Characteristics

Basic model.- Rudder tests of the basic configuration are presented in figure 13 for a thrust-coefficient range encountered during ground roll and take-off for rudder deflections up to approximately full design negative deflection ($\delta_{r_{max}} = -25^\circ$). Adequate rudder power is indicated for the low angle of attack (fig. 13(a)); however, full rudder would not be expected to provide trim at thrust coefficients above $T_c = 0.6$ for $\alpha = 11.4^\circ$ which corresponds roughly to the take-off attitude (fig. 13(b)).

The difficulty of attaining adequate directional control in the take-off condition is caused by the effects of slipstream rotation over the vertical tail which become more severe at higher angles of attack because of the greater vertical-tail area affected by the slipstream. The large flow angularity associated with slipstream rotation is shown in the tuft-grid photograph of figure 23(a) for the basic configuration, particularly near the base of the vertical tail. A number of devices were accordingly investigated in an attempt to counteract the effects of this flow angularity.

Modifications to the basic model.- The problem of attaining sufficient directional control at high thrust coefficients was anticipated



and provisions were made on the model for a skewed dive-brake arrangement and an adjustable vertical fin. Results of these modifications (figs. 14(a) and 14(b)) show insignificant improvements over the basic model. Similar unsuccessful results were obtained with the ventral and dorsal fins (figs. 14(c) and 14(d)) and with the increased rudder chord (fig. 14(e)).

An unpublished study of small fins placed ahead of a vertical tail showed that an appreciable sidewash effect on the vertical tail could be induced by a fin as small as 10 percent of the tail area. A triangular fin of this type was tested on the basic model and the results are presented in figure 15. Although some improvements were attained with the fin aligned with the thrust axis, these improvements were doubled by 20° deflection of a trailing-edge flap on the fin set opposite to the direction of slipstream rotation (fig. 15(a)). A comparison was made of the effect of fin flap deflection and fin incidence at the higher angle of attack (fig. 15(b)) and it is seen that the 20° flap deflection was essentially equivalent to a 10° fin incidence. Effectiveness of the triangular dorsal fin in reducing sidewash at the base of the vertical tail is shown in the tuft-grid photographs of figure 23(a) with the fin flap deflected 20° .

It is apparent that substantial improvements were achieved by use of the triangular fin; however, rudder power was still marginal above a thrust coefficient of unity at the highest angle of attack (fig. 15(b)).

Lateral-Stability Parameters

Power-on lateral-stability derivatives for the configurations with the wing flaps retracted and deflected are presented in figures 16 and 17, both with and without the tail surfaces. These stability parameters were obtained by assuming a linear variation between $\beta = \pm 5^\circ$; of course, the significance of the parameters is decreased where nonlinearities are present through zero sideslip (see rolling-moment coefficients plotted in figs. 19(b) and 20(b)).

Dihedral effect.- Negative dihedral effect is indicated through the lift range without the tail for both flap configurations (figs. 16 and 17(a)). Addition of the tail, with flaps retracted, afforded an appreciable favorable dihedral effect at low lift which is in agreement with the tail increment obtained with the wing off (fig. 18(b), propeller off). Above a lift coefficient of unity, negative dihedral effect is indicated with flaps retracted; it should be noted, however, that these high-lift results (fig. 16) were obtained with the controls neutral and the model was considerably out of trim, both laterally and directionally (see fig. 8). Effects of rudder deflection are shown in figure 17(a)

with $\delta_F = 40^\circ$ and the characteristics with the model more nearly in directional trim were markedly different from those obtained with the rudder neutral. It is believed, therefore, that the significance of the power-on lateral-stability parameters presented is decreased at high lift where appreciable aileron and rudder deflections were required for trim.

Directional stability.- The directional stability at low lift with the tail on is high and decreases considerably at high lift with controls neutral (figs. 16 and 17). This loss at high lift encountered with the propeller off (ref. 1) was found to be associated with the fuselage wake; whereas, with the propeller operating it would be expected for this type of airplane arrangement that the slipstream would provide increasing tail effectiveness for constant-power operation. Results with the rudder deflected (fig. 17(a)) show very high directional stability throughout the lift range. This difference in results with the rudder deflected suggests the possibility that the vertical tail may have been near maximum lift with neutral rudder. This behavior is also indicated in the sideslip results of figure 20(b) for neutral rudder where $C_{n\beta}$ is negative for negative sideslip angles.

Sideslip Characteristics

Results of a few tests made through a range of sideslip angles are presented in figures 18 to 21. An interesting effect was observed with the propeller-fuselage combination which is not generally encountered in complete-model tests. Longitudinal characteristics (fig. 18(a)) show a large variation of lift with sideslip angle when the propeller was operating. This lift variation arises from slipstream rotation over the yawed fuselage and could be estimated accurately up to $\pm 10^\circ$ sideslip by the method of reference 4. Addition of the wing with flaps retracted (fig. 19(a)) essentially eliminated this slipstream effect.

Power-on yawing-moment results of the complete model with the tail on ($T_c = 0.66$, fig. 19(b)) indicate a marked decrease in $C_{n\beta}$ as the sideslip angle varied from positive to moderate negative sideslip angles. This behavior was found from a survey to be associated with a loss in dynamic pressure as the vertical tail emerged from the slipstream, and at negative sideslip angles greater than -4° , the vertical tail was in essentially free-stream dynamic pressure.

Rolling-moment results of the complete model (fig. 19(b)) appear erratic at low sideslip angles and repeatability of test points was poor in some instances. The sensitivity of this wing to small flow changes was also indicated in the rolling-moment results of reference 1. The

low Reynolds number of the present tests could have affected the rolling-moment behavior in sideslip.

Characteristics in sideslip for the flap-deflected configuration are presented in figures 20 and 21 and some of the curves of figure 20 are given in figure 21 for comparison. Some tests were made in order to study further the effects of the triangular fin which was found beneficial for directional trim with power on (fig. 21). The over-all fin effect on directional trim amounted to about 12° of additional rudder deflection at zero sideslip. This favorable over-all fin effect on yawing moments was due to a large reduction in sidewash over the tail with the fin on. All of this favorable sidewash effect, of course, was not indicated in the tail-on results because the fin was located behind the moment reference and the direct forces on the fin produced moments which were unfavorable (see tail-off results, fig. 21(b)).

A few tuft-grid photographs are presented in figures 23(b) and 23(c) to show the flow field behind the model at fairly large sideslip angles. The extent of the slipstream with $T_c = 0.66$ (fig. 23(b)) is obscured by the presence of a strong vortex which intersects the tuft grid near the tip of the horizontal-tail location. The origin of this vortex was not determined and the vortex was found both with the flaps retracted and deflected for the propeller-windmilling condition at large sideslip angles. Inasmuch as the vortex did not appear to be associated with propeller slipstream, this vortex may possibly have come from the canopy.

CONCLUSIONS

Results of a low-speed investigation of the static lateral stability and control characteristics of a $1/6$ -scale model of the Republic XF-84H airplane with the propeller operating have indicated the following conclusions:

1. Serious aileron- and rudder-control deficiencies were evident at high angles of attack with the propeller operating. These problems appeared to be associated with the aerodynamic asymmetry induced by propeller slipstream rotation and could be alleviated by reducing rotation effects or by providing appropriate asymmetry of control deflections.
2. With full power on and flaps retracted, full aileron deflection would not be expected to provide lateral trim much above $\alpha = 12^\circ$. Projection of only the left slat was very effective in alleviating the left-wing roll-off tendency with power on. The use of differential wing-flap deflection also appeared to offer a promising means of alleviating power-on lateral-control difficulties.

3. Full design negative rudder deflection would not be expected to provide directional trim in the take-off attitude at thrust coefficients above $T_c = 0.60$. The only effective device found to alleviate this problem was a small triangular dorsal fin located between the canopy and vertical tail and oriented opposite to the direction of slipstream rotation to reduce adverse sidewash effects on the tail.

4. Although significant benefits were realized with several modifications, none of those tested would be expected to afford satisfactory behavior for all normal flight conditions.

Langley Aeronautical Laboratory,
National Advisory Committee for Aeronautics,
Langley Field, Va., June 12, 1953.

Joseph Weil
for William C. Sleeman, Jr.
Aeronautical Research Scientist

William D. Morrison, Jr.
Aeronautical Research Scientist

Approved:

Thomas A. Harris

Thomas A. Harris
Chief of Stability Research Division

lc

REFERENCES

1. Weil, Joseph, Sleeman, William C., Jr., and Byrnes, Andrew L., Jr.: Investigation of the Effects of Wing and Tail Modifications on the Low-Speed Stability Characteristics of a Model Having a Thin 40° Swept Wing of Aspect Ratio 3.5. NACA RM L53C09, 1953.
2. Sleeman, William C., Jr., and Byrnes, Andrew L., Jr.: Low-Speed Longitudinal Stability Characteristics of a 1/6-Scale Model of the Republic XF-84H Airplane With the Propeller Operating. NACA RM SL53F26, U. S. Air Force, 1953.
3. Gillis, Clarence L., Polhamus, Edward C., and Gray, Joseph L., Jr.: Charts for Determining Jet-Boundary Corrections for Complete Models in 7- by 10-Foot Closed Rectangular Wind Tunnels. NACA WR, L-123, 1945. (Formerly NACA ARR L5G31.)
4. Ribner, Herbert S., and MacLachlan, Robert: Effect of Slipstream Rotation in Producing Asymmetric Forces on a Fuselage. NACA TN 1210, 1947.

TABLE I

SUMMARY OF BASIC MODEL GEOMETRY

Wing:	
Area (not including inlet area), sq ft	9.03
Span, ft	5.59
Sweepback of quarter-chord line, deg	40
Aspect ratio	3.45
Taper ratio	0.578
Dihedral	-3° 30'
Incidence	2° 30'
Geometric twist, deg	0
Mean aerodynamic chord, ft	1.67
Airfoil section (normal to quarter-chord line)	NACA 64A010
Root chord, ft	2.063
Tip chord, ft	1.195
Flap:	
Type	Plain trailing edge
Area (one flap), sq ft	0.420
Span, ft	1.009
Hinge line, percent c	75
Maximum deflection, deg	40
Aileron:	
Area (one aileron) sq ft	0.38
Span, ft	1.24
Hinge line, percent c	75
Maximum deflection (normal to hinge line), deg	±18
Leading-edge slat:	
Span of one slat (normal to model center line), ft	1.33
Ratio of slat chord to wing chord (normal to c/4)	0.140
Inboard edge (from model center line), ft	1.347
Forward extension of slat, percent c	8.4
Downward extension of slat, percent c	7.24
Horizontal tail:	
Type	All-movable
Area, sq ft	1.55
Span, ft	2.36
Sweepback (quarter-chord line), deg	40
Aspect ratio	3.59
Taper ratio	1.0
Dihedral, deg	0
Chord, ft	0.67
Deflection range, deg	-6 to 15
Airfoil section (normal to leading edge)	NACA 64A009
Tail length (center of gravity to quarter mean aerodynamic chord of horizontal tail), ft	3.808
Vertical tail:	
Area, sq ft	1.73
Span, ft	1.815
Sweepback of quarter-chord line	41° 16' 10"
Aspect ratio	1.90
Taper ratio	0.340
Mean aerodynamic chord	0.955
Airfoil section (normal to quarter chord line)	NACA 64(10)A011

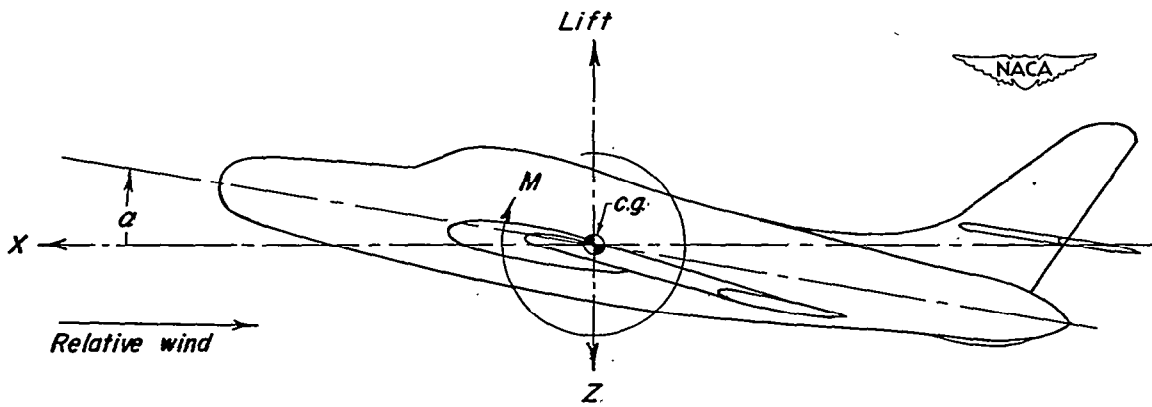
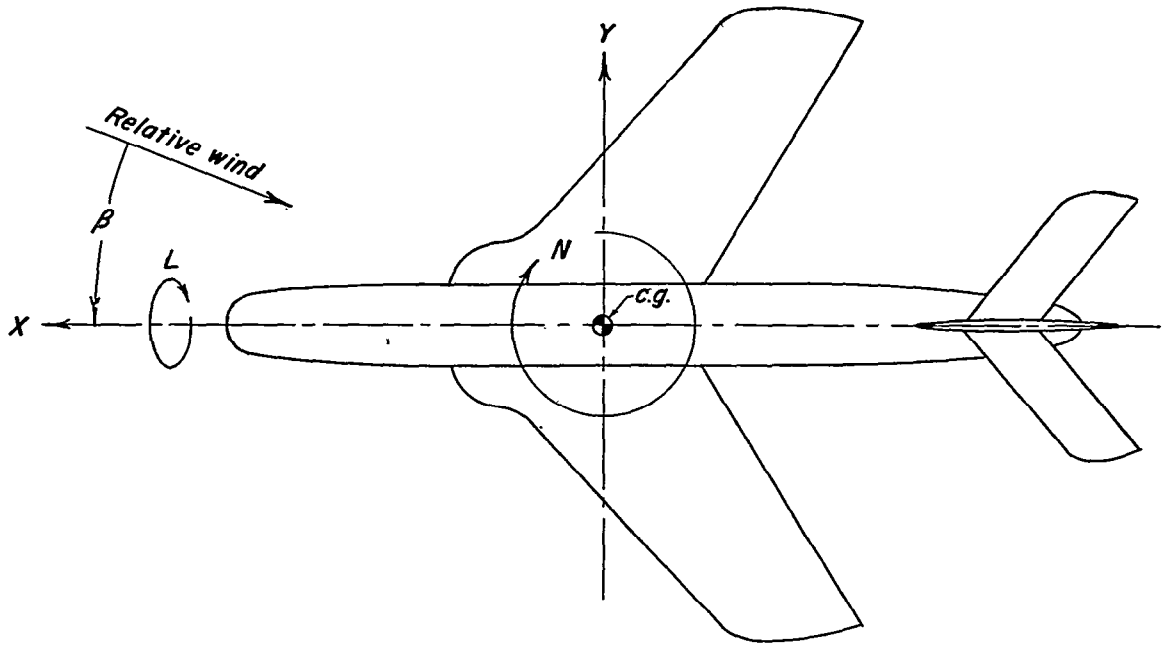
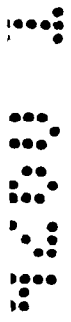


Figure 1.- System of axes and control-surface deflections. Positive values of forces, moments, and angles are indicated by arrows.

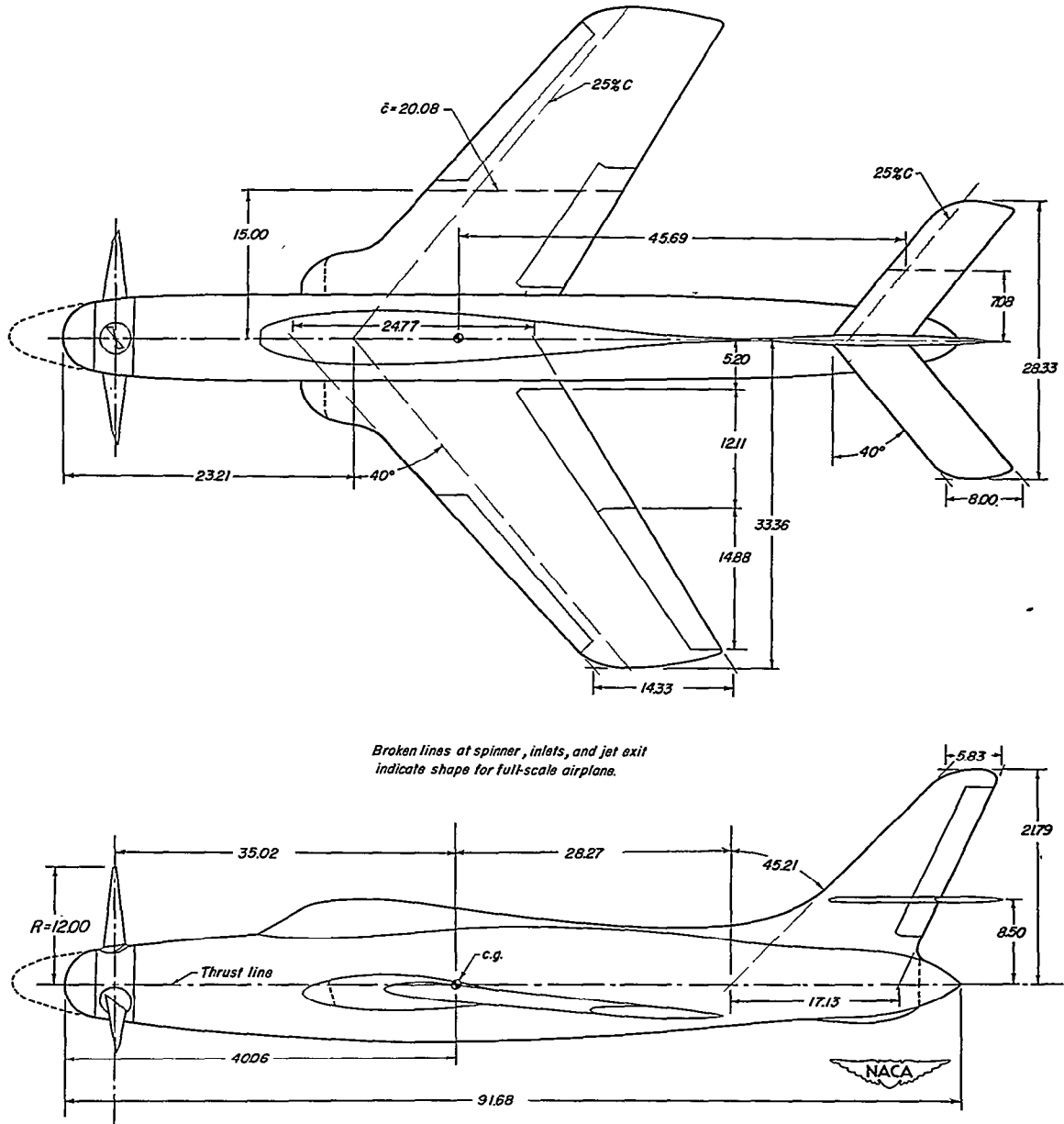
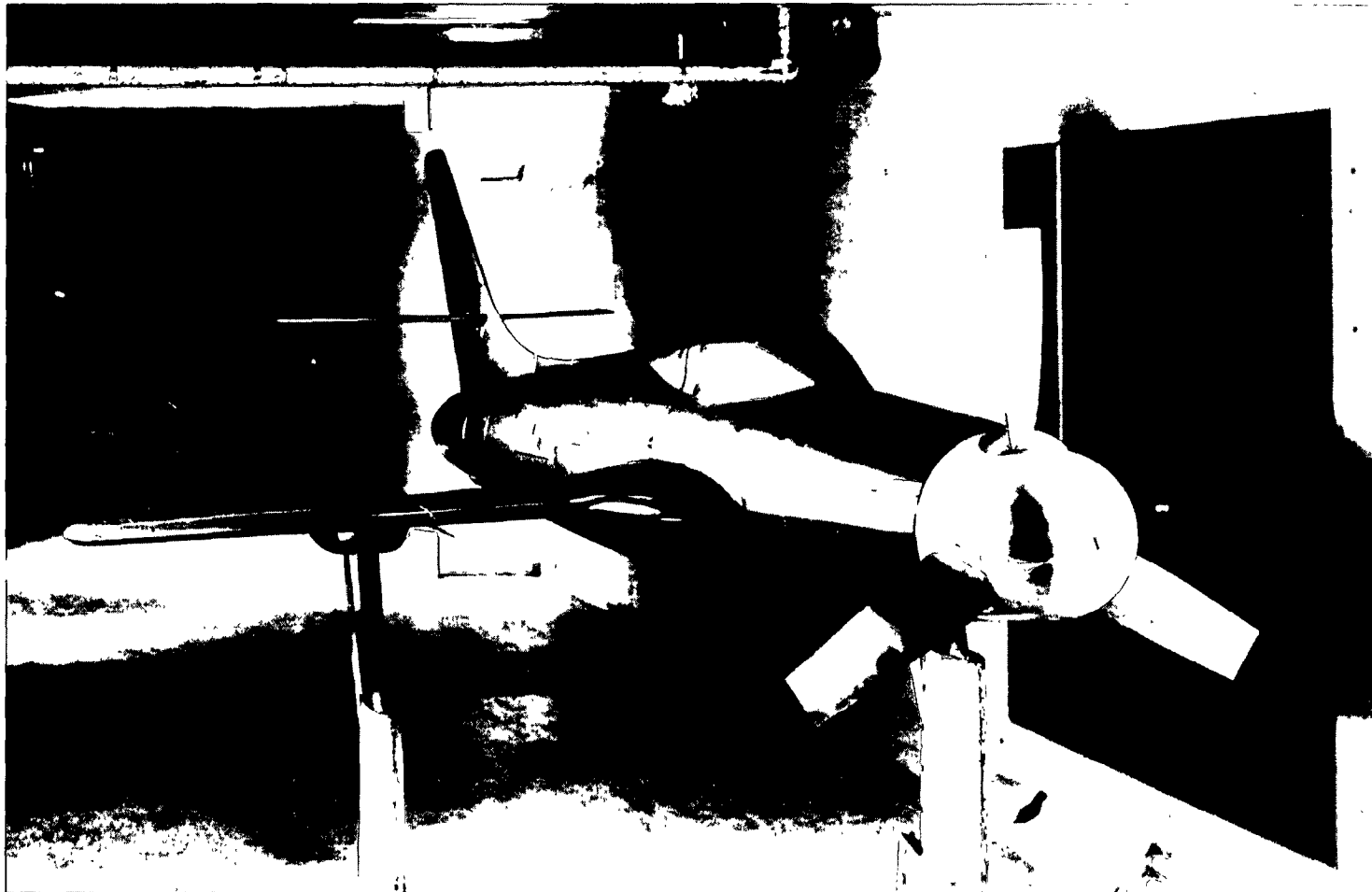


Figure 2.- Two-view drawing of 1/6-scale model of the original Republic XF-84H airplane configuration. All dimensions are in inches.



L-75003

Figure 3.- Photograph of the 1/6-scale model of the original Republic XF-84H airplane configuration mounted in the Langley 300 MPH 7- by 10-foot tunnel.

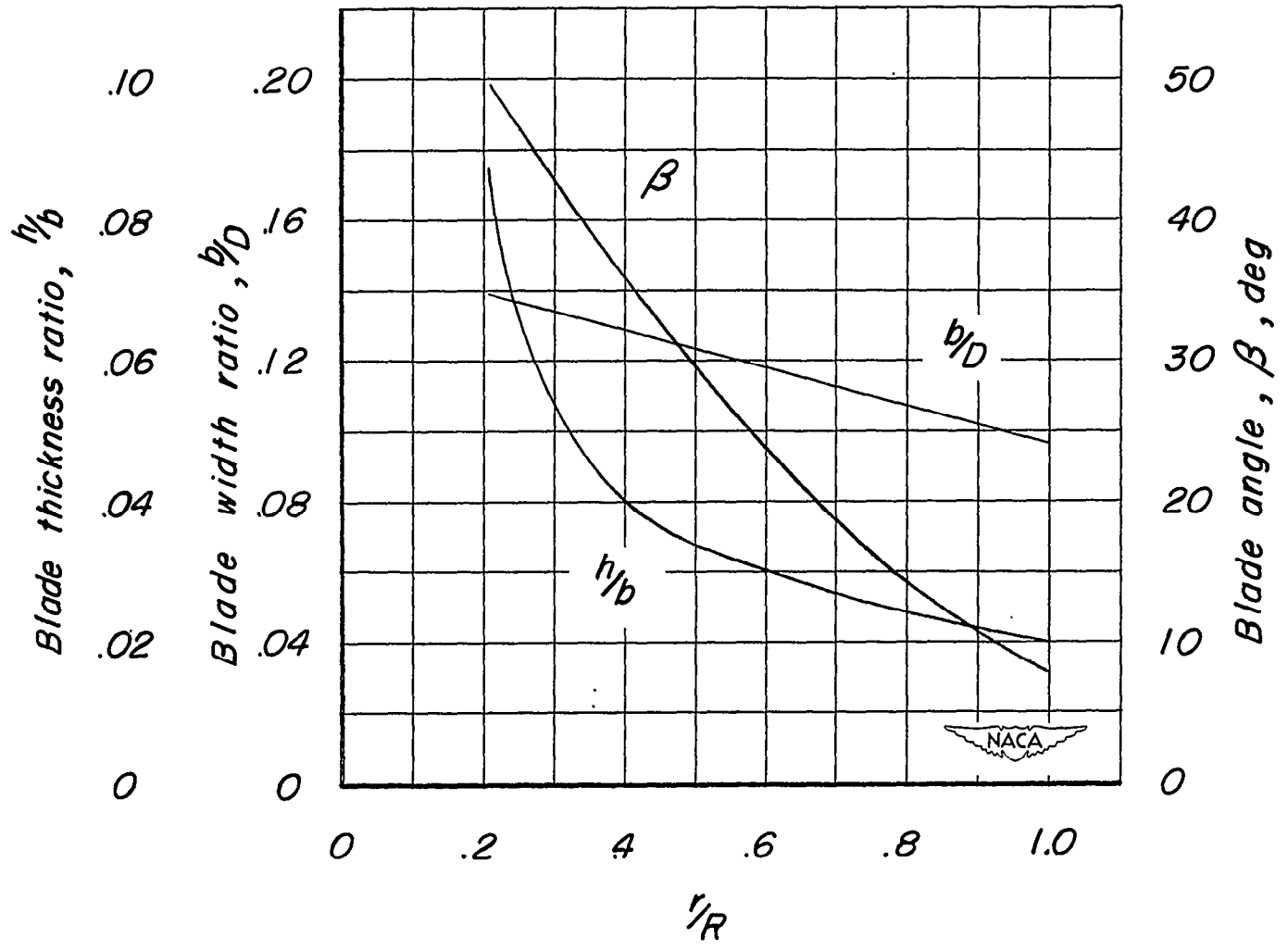


Figure 4.- Blade-form characteristics of the model propeller.

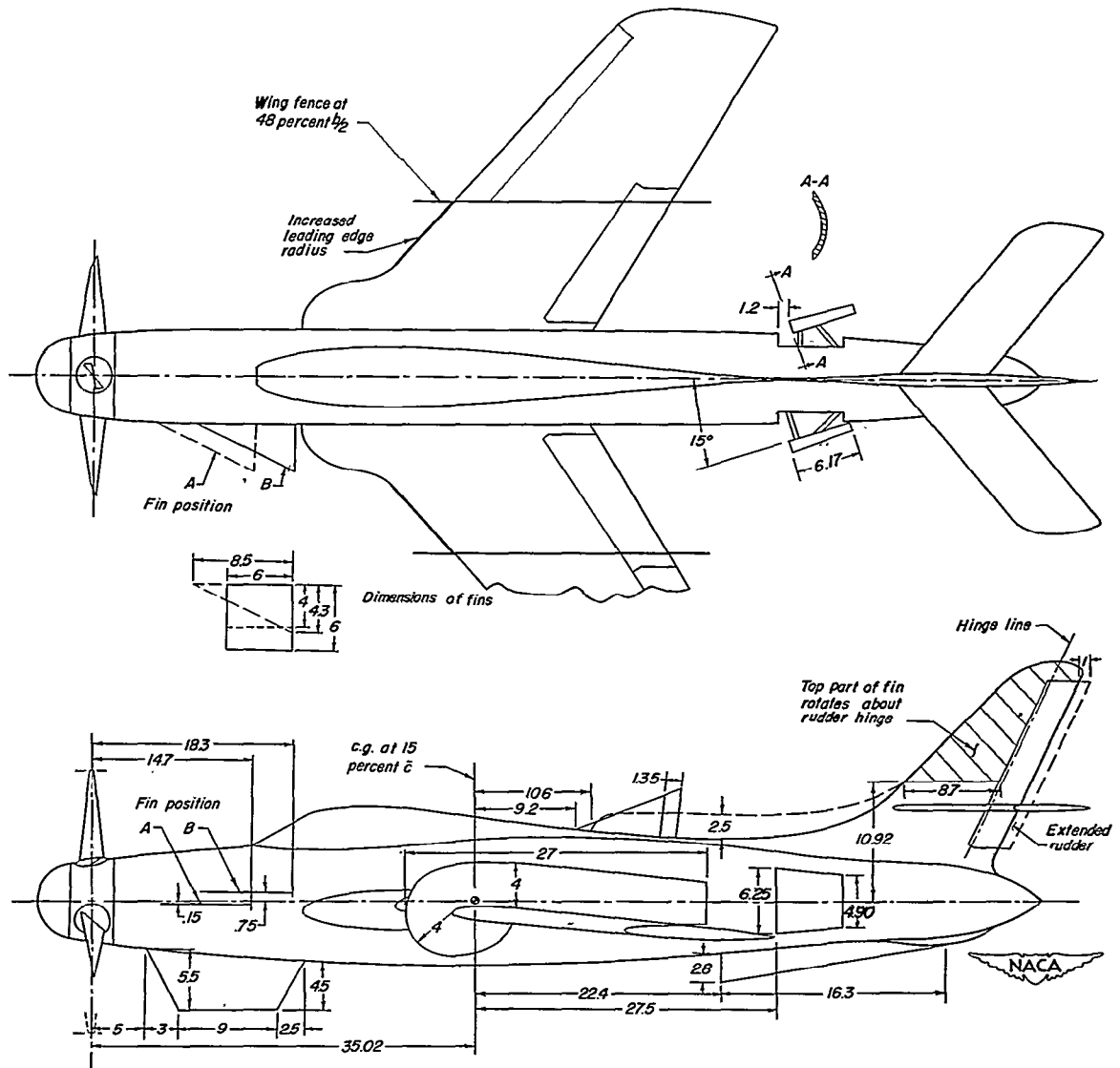


Figure 5.- Details of various devices tested to improve the characteristics of the basic configuration. All dimensions are in inches.

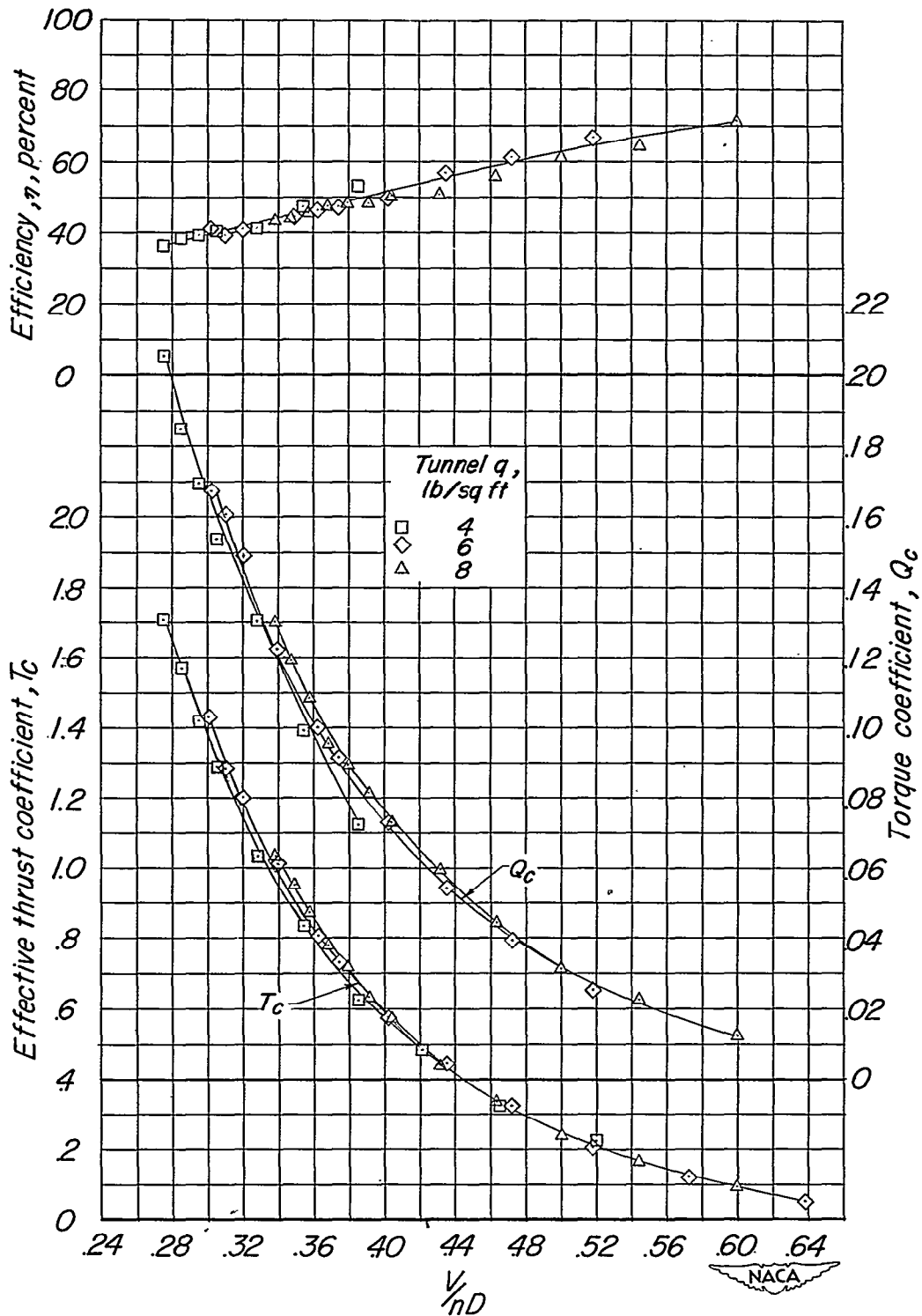


Figure 6.- Characteristics of the model propeller as determined from calibrations with the propeller on the basic fuselage. Wing, tail, canopy, and external protuberances removed. $\beta_{0.75R} = 16.5^\circ$.

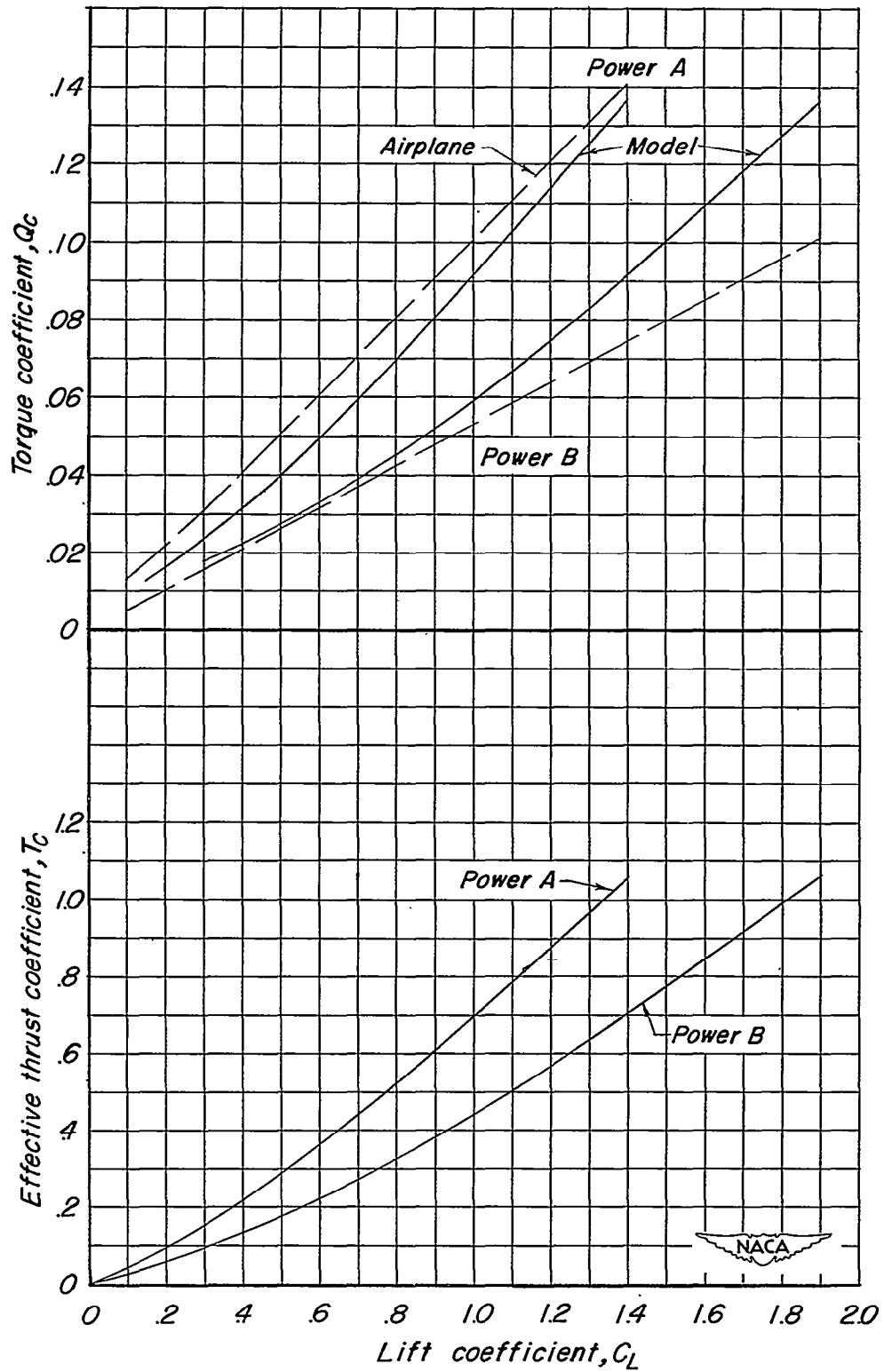


Figure 7.- Variation of effective-thrust and torque coefficients with lift coefficient for the constant-power conditions investigated.

- Power A
- ◇ $T_c = 0.22$
- Propeller windmilling

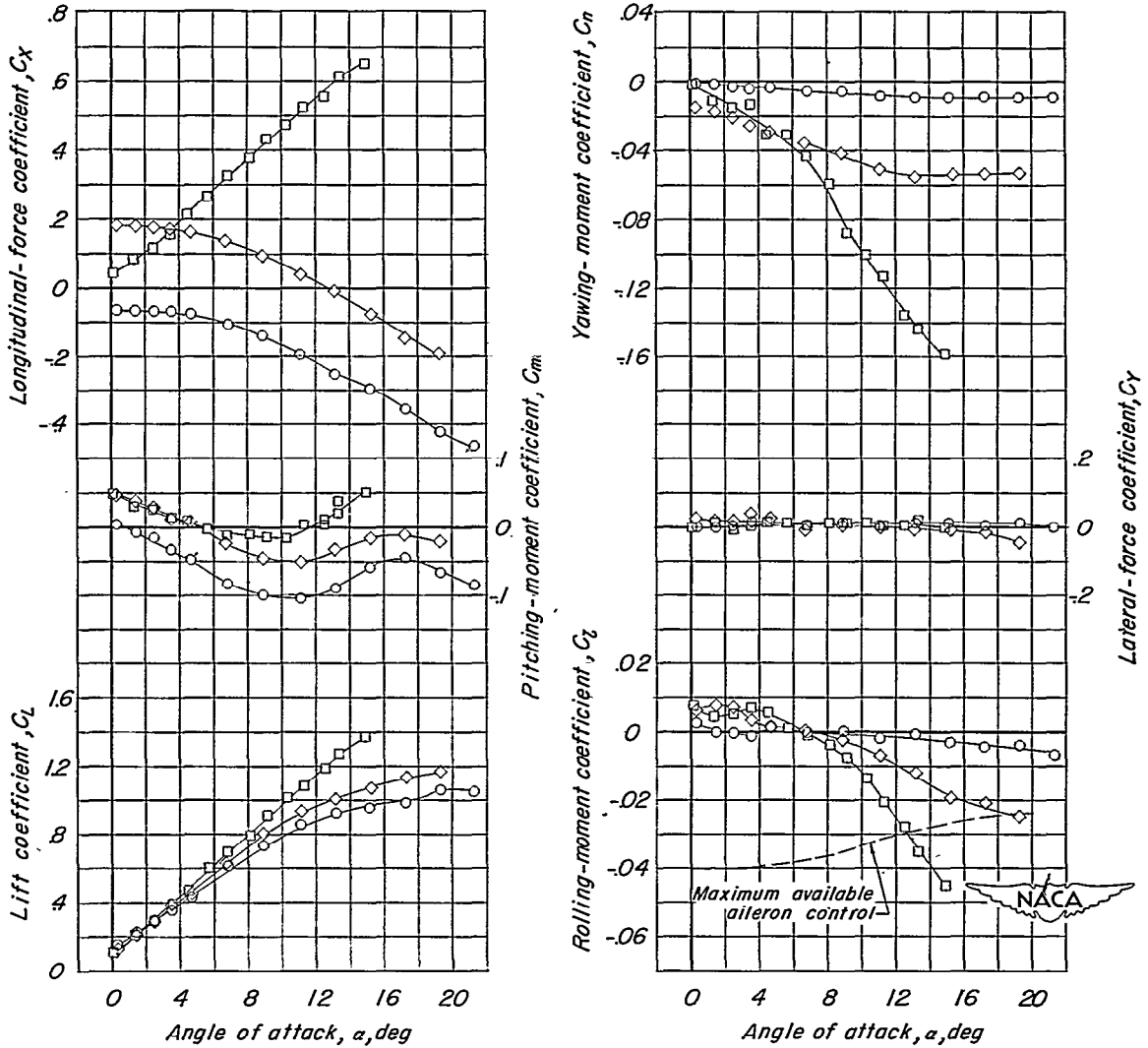
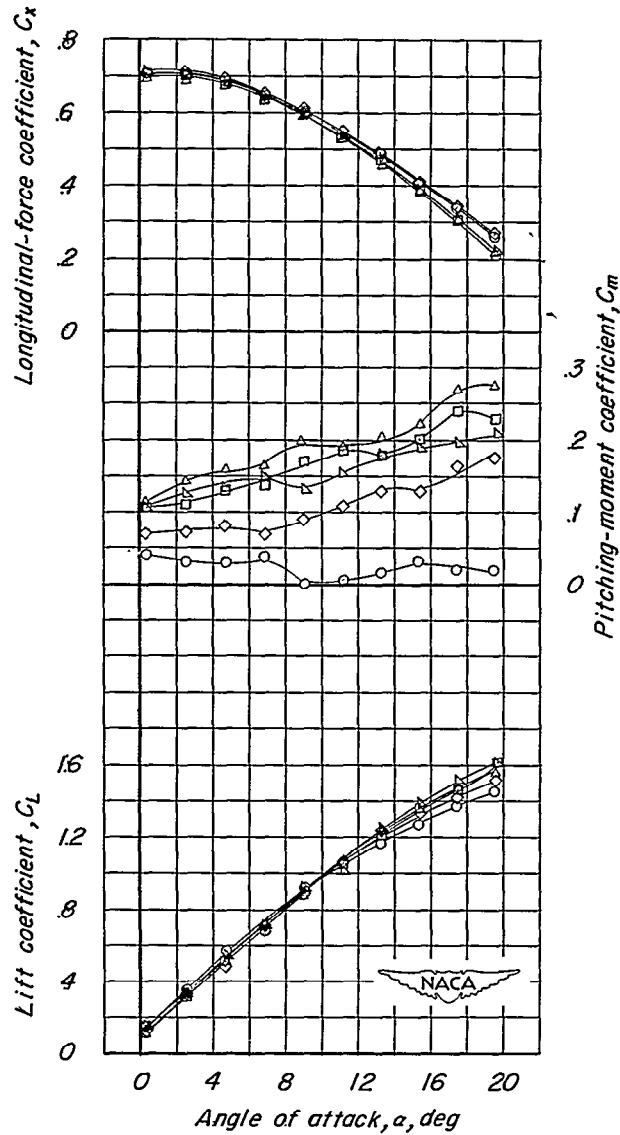
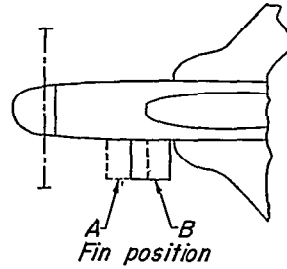


Figure 8.- Typical effects of propeller operation on the aerodynamic characteristics of the basic configuration for zero sideslip.
 $\delta_f = 0^\circ$; $q = 8$ lb/sq ft.

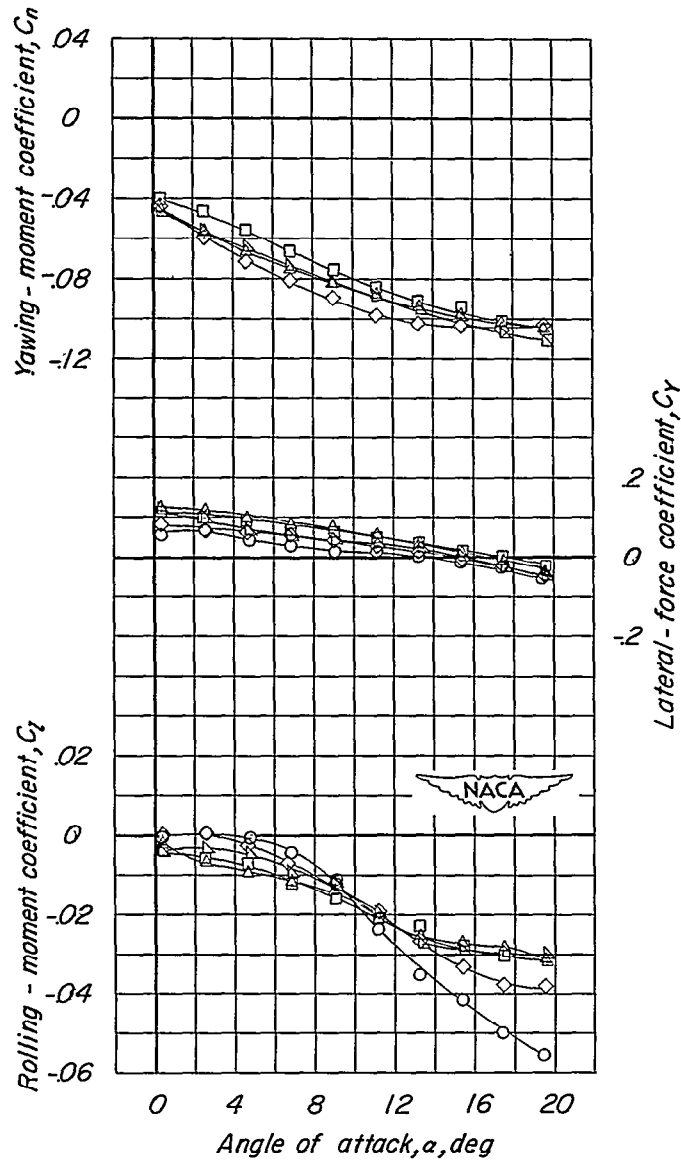
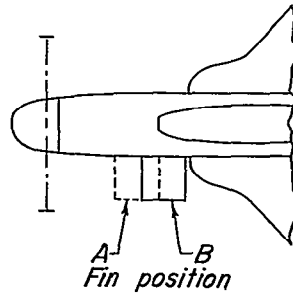
Fin span, in	Fin position	Fin incidence, deg
—	○ Off	—
6	△ A	10 (nose down)
6	□ B	0
6	◇ B	10 (nose down)
4	△ A	0



(a) Longitudinal characteristics.

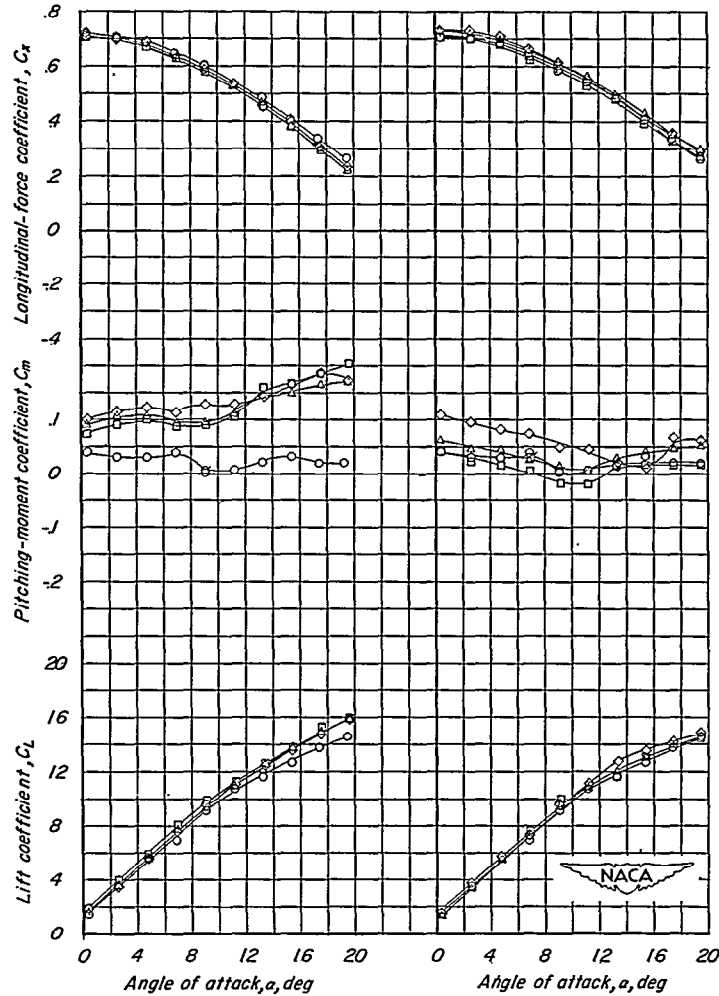
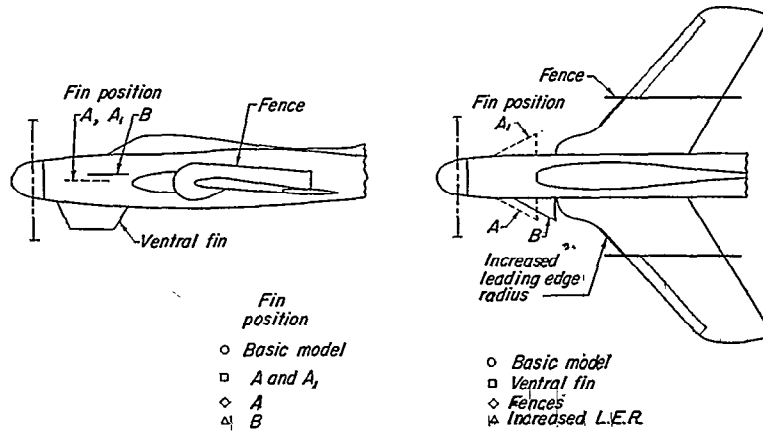
Figure 9.- Effect of a rectangular fin located ahead of the wing on the characteristics with the propeller operating. $\delta_f = 0^\circ$; $T_c = 0.81$; $i_t = \delta_a = \delta_r = 0^\circ$; $q = 8$ lb/sq ft.

Fin span, in.	Fin position	Fin incidence, deg
—	○ Off	—
6	△ A	10 (nose down)
6	□ B	0
6	◇ B	10 (nose down)
4	△ A	0



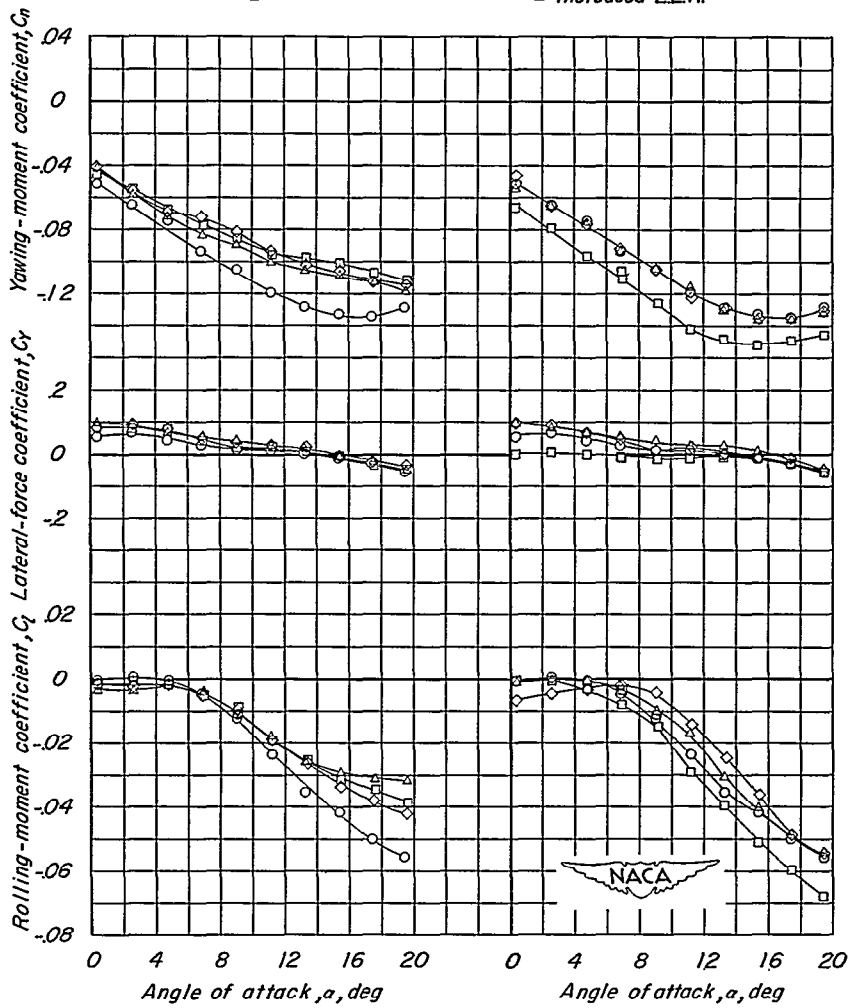
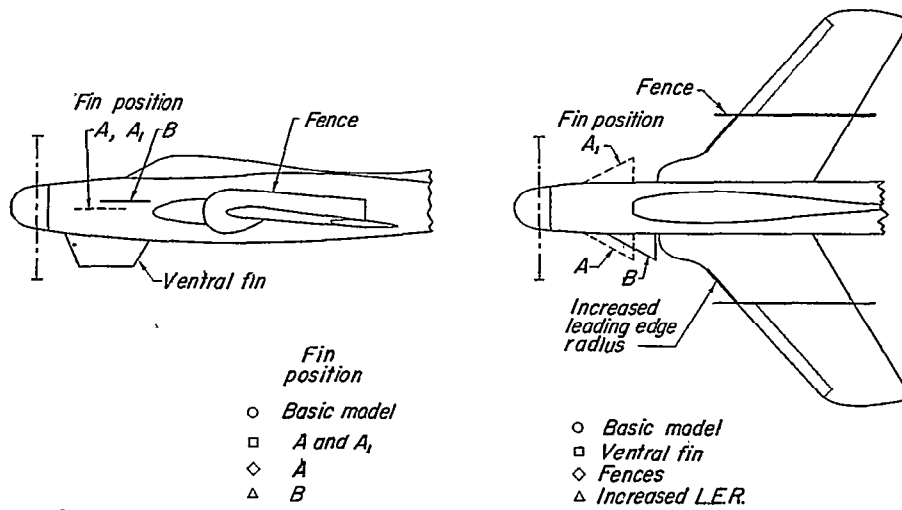
(b) Lateral characteristics.

Figure 9.- Concluded.



(a) Longitudinal characteristics.

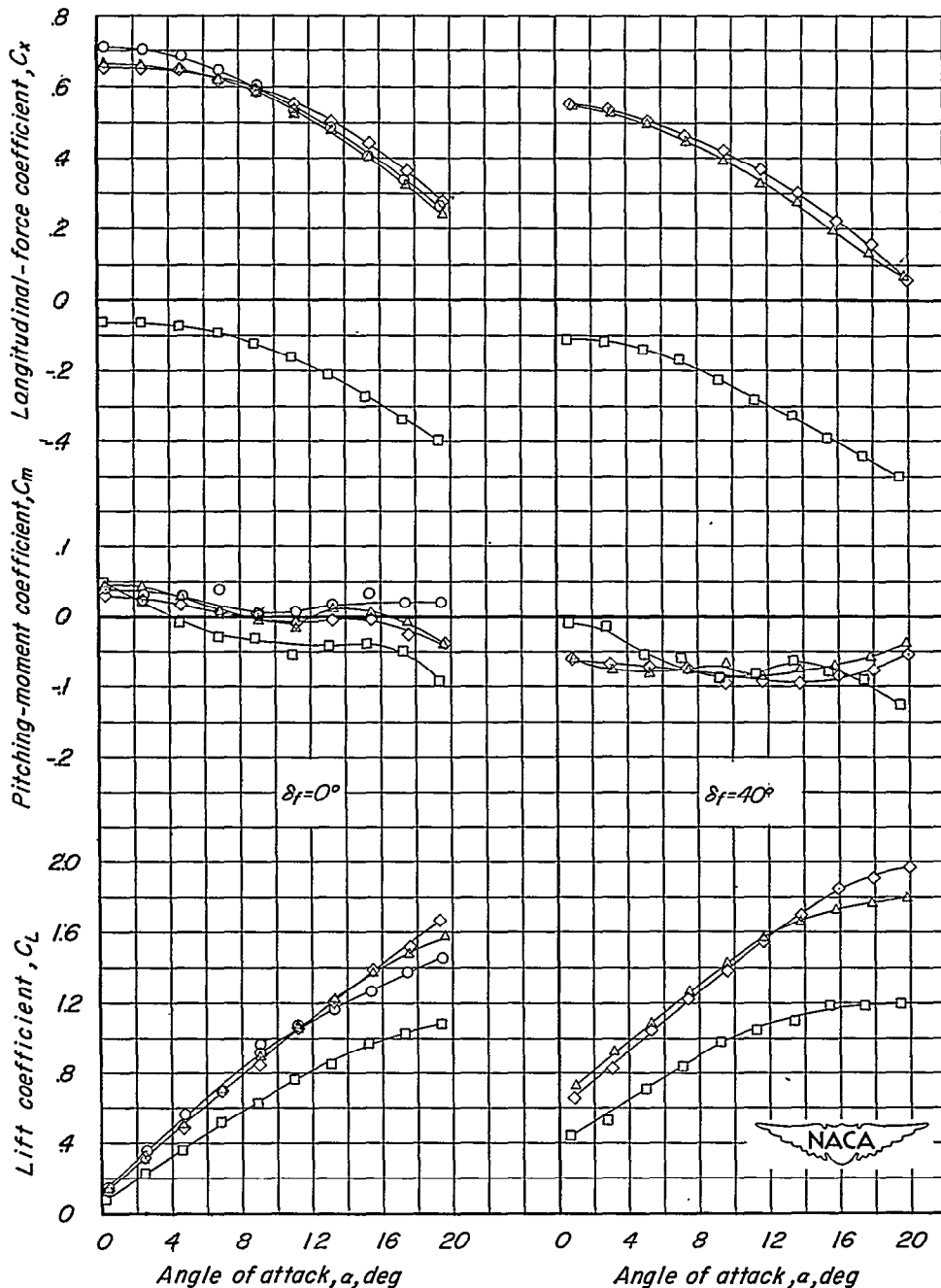
Figure 10.- Effect of several devices investigated to improve lateral trim characteristics with the propeller operating. $\delta_F = 0^\circ$; $T_C = 0.81$; $i_t = \delta_r = 0^\circ$; $q = 8 \text{ lb/sq ft}$.



(b) Lateral characteristics.

Figure 10.- Concluded.

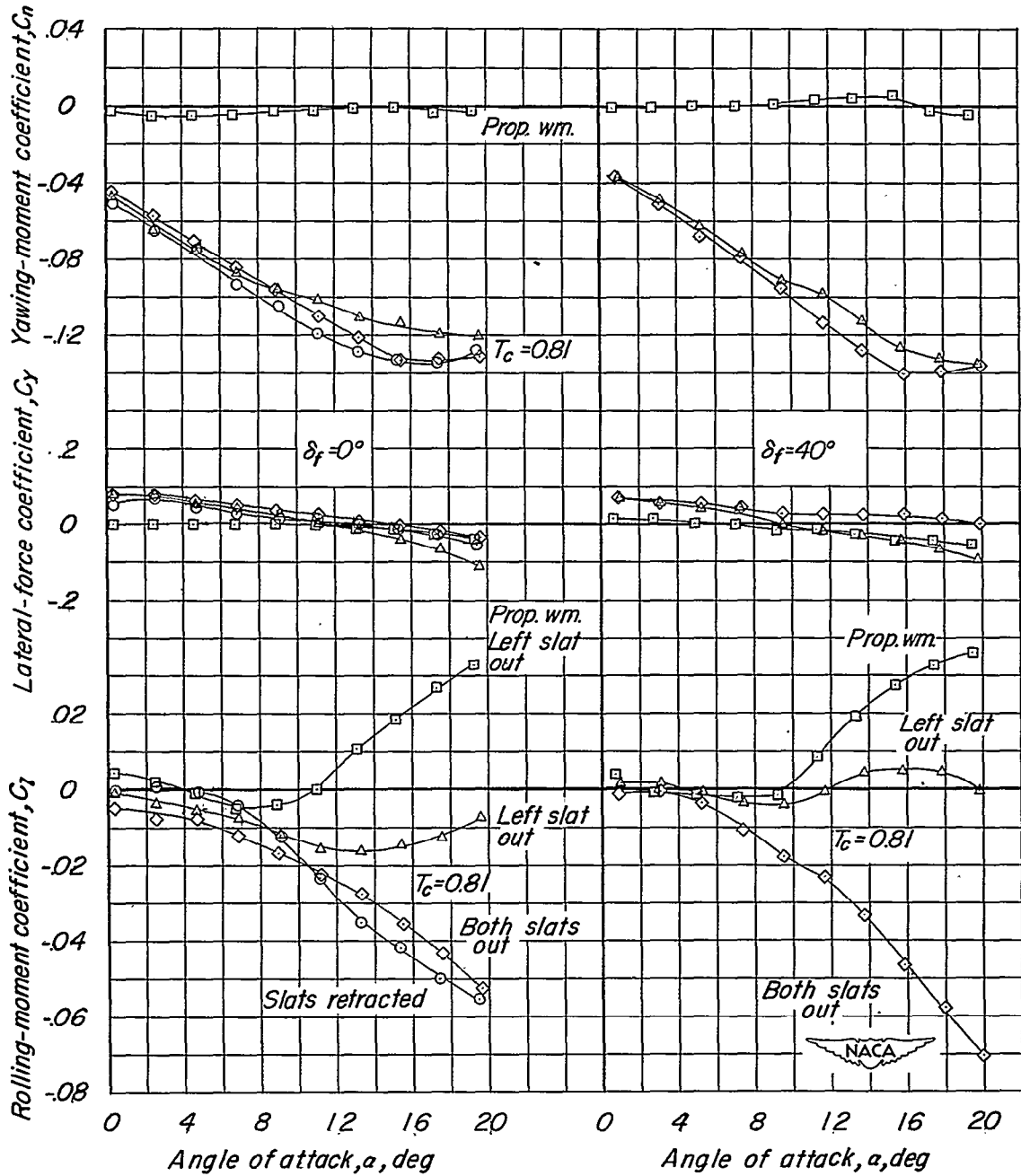
- Slats retracted; $T_c = 0.81$
- Left slat out; Propeller windmilling
- △ Left slat out; $T_c = 0.81$
- ◇ Both slats out; $T_c = 0.81$



(a) Longitudinal characteristics.

Figure 11.- Effect of deflecting both slats and only the left slat with and without the propeller operating. $i_t = \delta_r = \delta_a = 0^\circ$; $q = 8$ lb/sq ft.

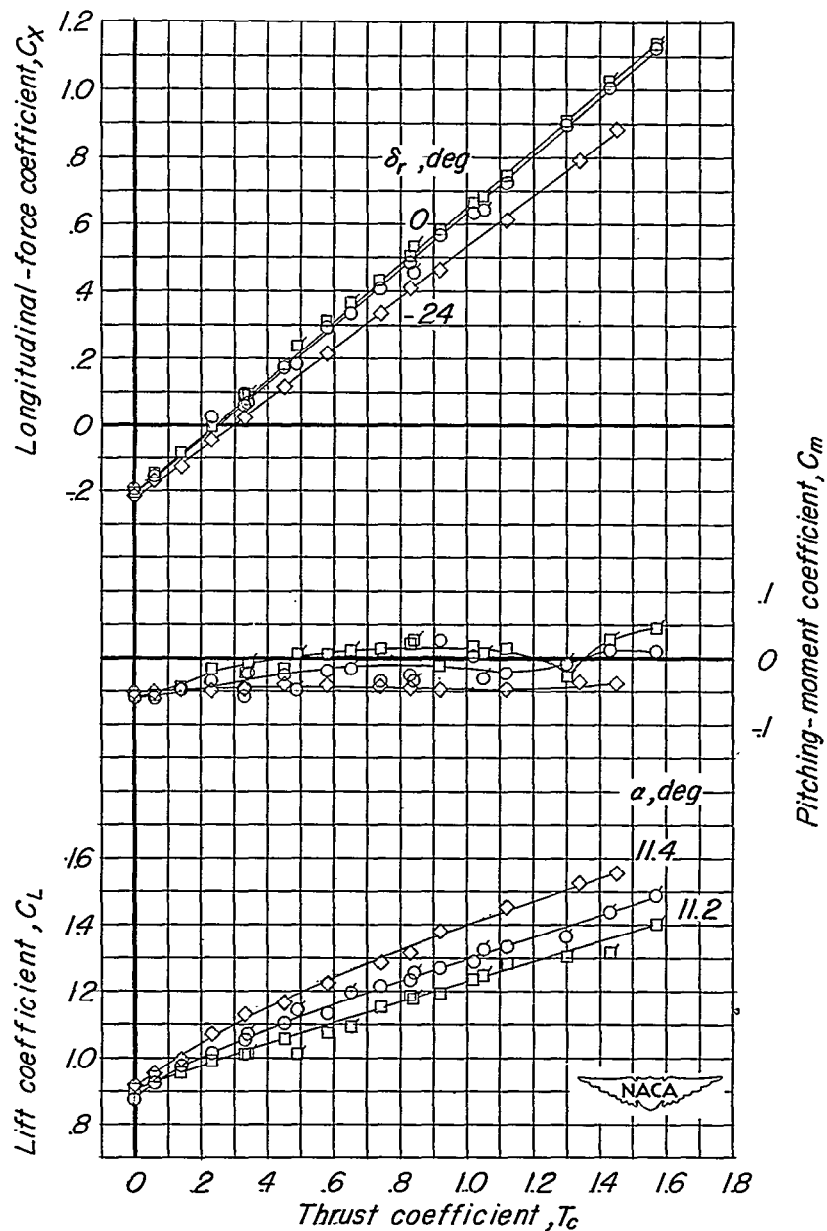
- Slats retracted; $T_c=0.81$
- Left slat out; Propeller windmilling
- △ Left slat out; $T_c=0.81$
- ◇ Both slats out; $T_c=0.81$



(b) Lateral characteristics.

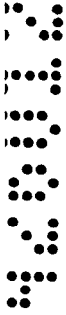
Figure 11.- Concluded.

δ_L, deg	δ_R, deg	
0	20	○
20	0	□
20	20 Left slat out	◇

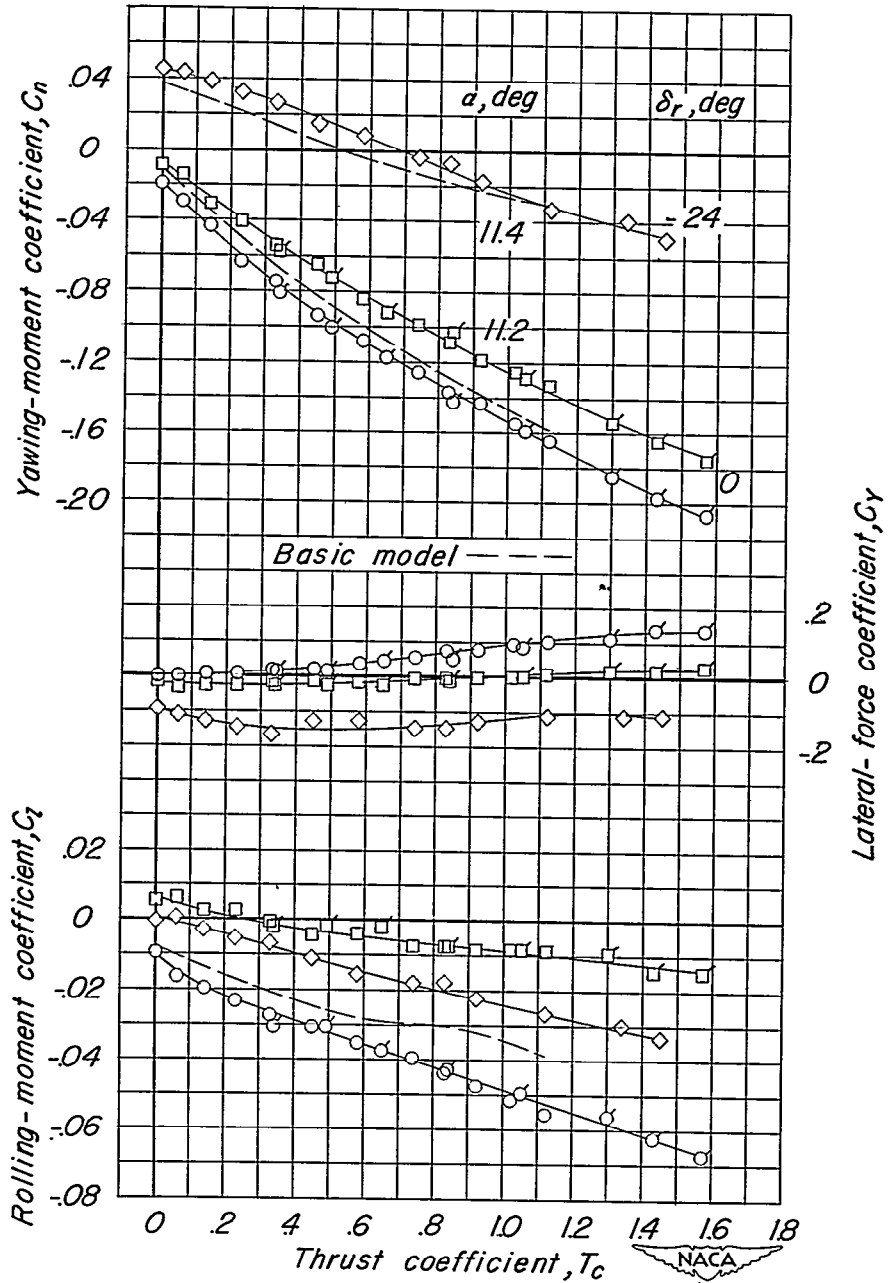


(a) Longitudinal characteristics.

Figure 12.- Effect of asymmetric flap deflection and slat deflection at a constant angle of attack with the propeller operating. $i_t = \delta_a = 0^\circ$; $q = 6 \text{ lb/sq ft}$. (Flagged symbols indicate data at $q = 4 \text{ lb/sq ft}$.)

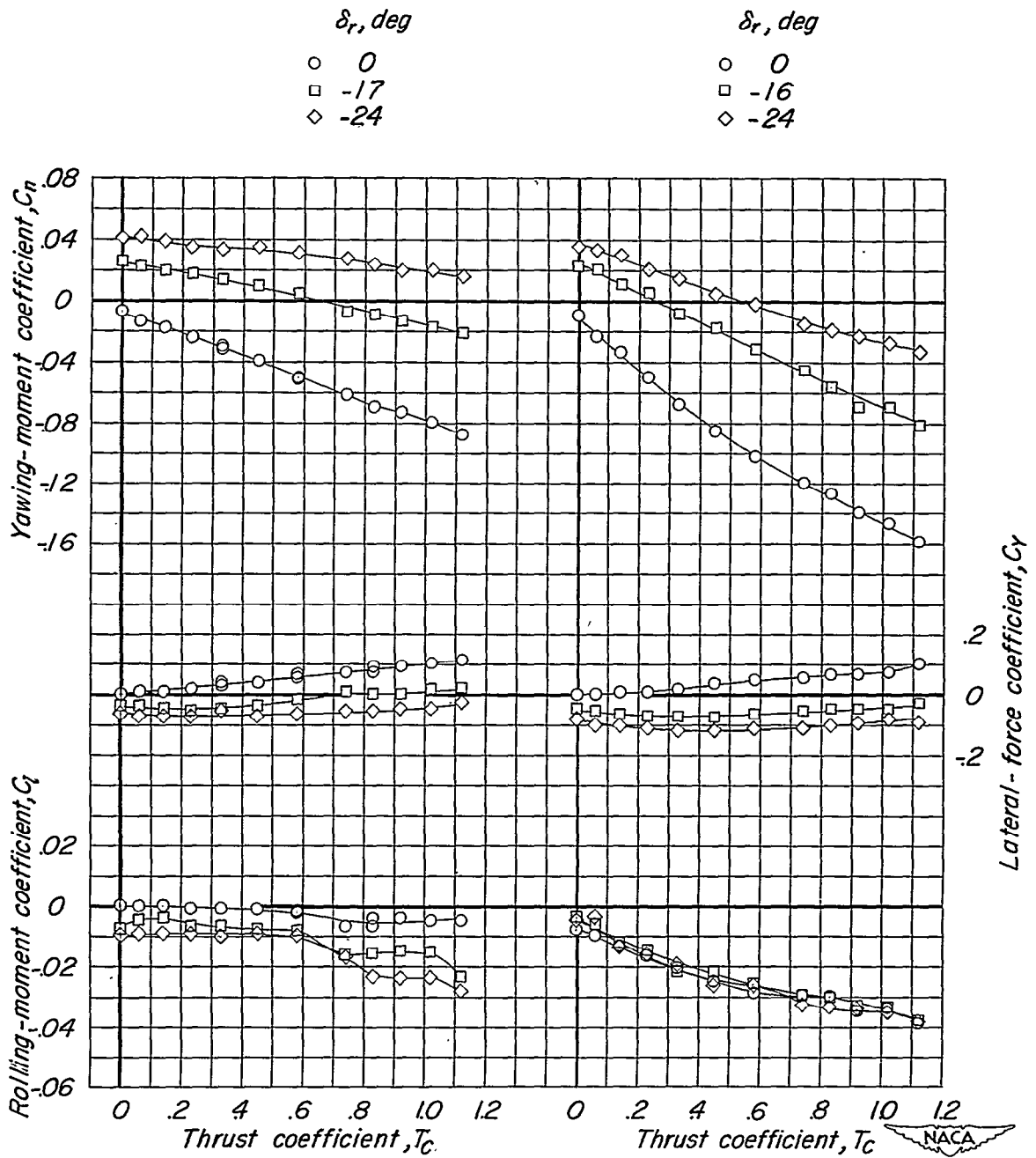


δ_{f_L}, deg	δ_{f_R}, deg	
0	20	○
20	0	□
20	20	Left slat out ◇



(b) Lateral characteristics. Dashed curves for the basic model; $\delta_{f_L} = \delta_{f_R} = 20^\circ$; $i_t = \delta_r = \delta_a = 0^\circ$; both slats out.

Figure 12.- Concluded.

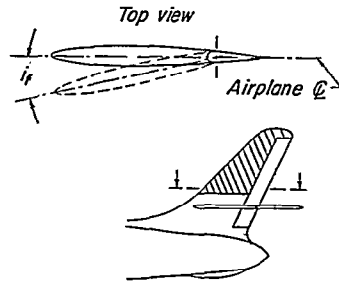
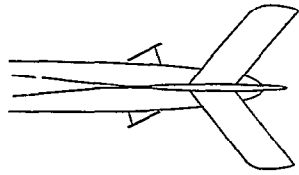
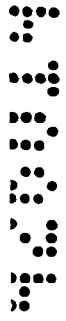


(a) $\alpha = 2.8^\circ$.

(b) $\alpha = 11.4^\circ$.

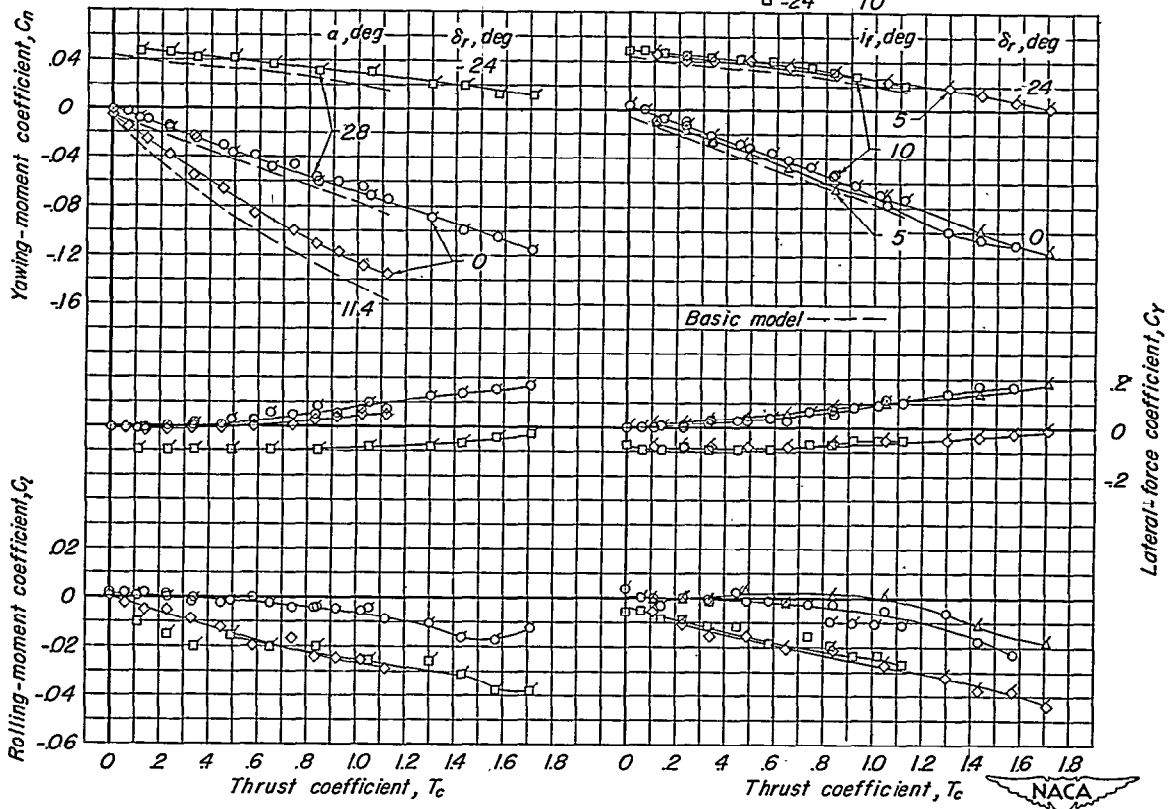
Figure 13.- Directional trim characteristics of the basic model with the rudder deflected. $\delta_r = 20^\circ$; $i_t = \delta_a = 0^\circ$; slats extended; $q = 6 \text{ lb/sq ft.}$ (Flagged symbols indicate data at $q = 4 \text{ lb/sq ft.}$)

~~CONFIDENTIAL~~



α, deg	δ_r, deg
○ 2.8	0
□ 2.8	-24
◇ 11.4	0

δ_r, deg	i_t, deg
△ 0	5
◇ -24	5
○ 0	10
□ -24	10

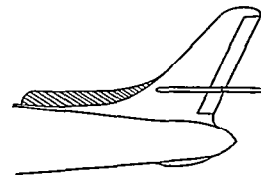
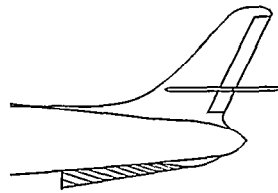


(a) Dive brakes.

(b) Vertical fin offset.
 $\alpha = 2.8^\circ$.

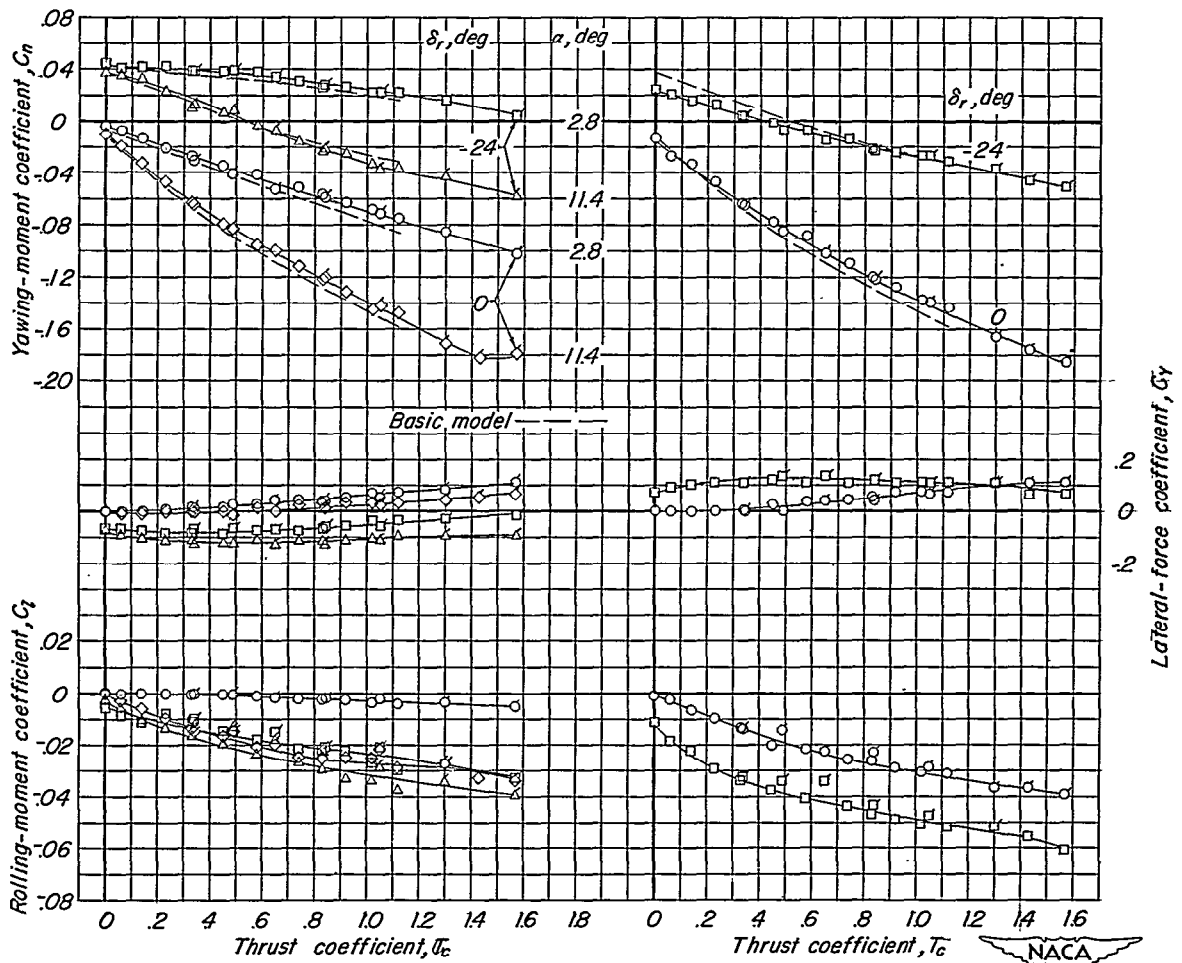
Figure 14.- Effects of various modifications investigated to improve the directional trim characteristics of the basic model. $\delta_f = 20^\circ$; $i_t = \delta_a = 0^\circ$; slats extended; $q = 6 \text{ lb/sq ft}$. (Flagged symbols indicate data at $q = 4 \text{ lb/sq ft}$.)

~~CONFIDENTIAL~~



δ_r, deg	α, deg
○	2.8
◇	11.4
□	2.8
△	11.4

δ_r, deg
○
□



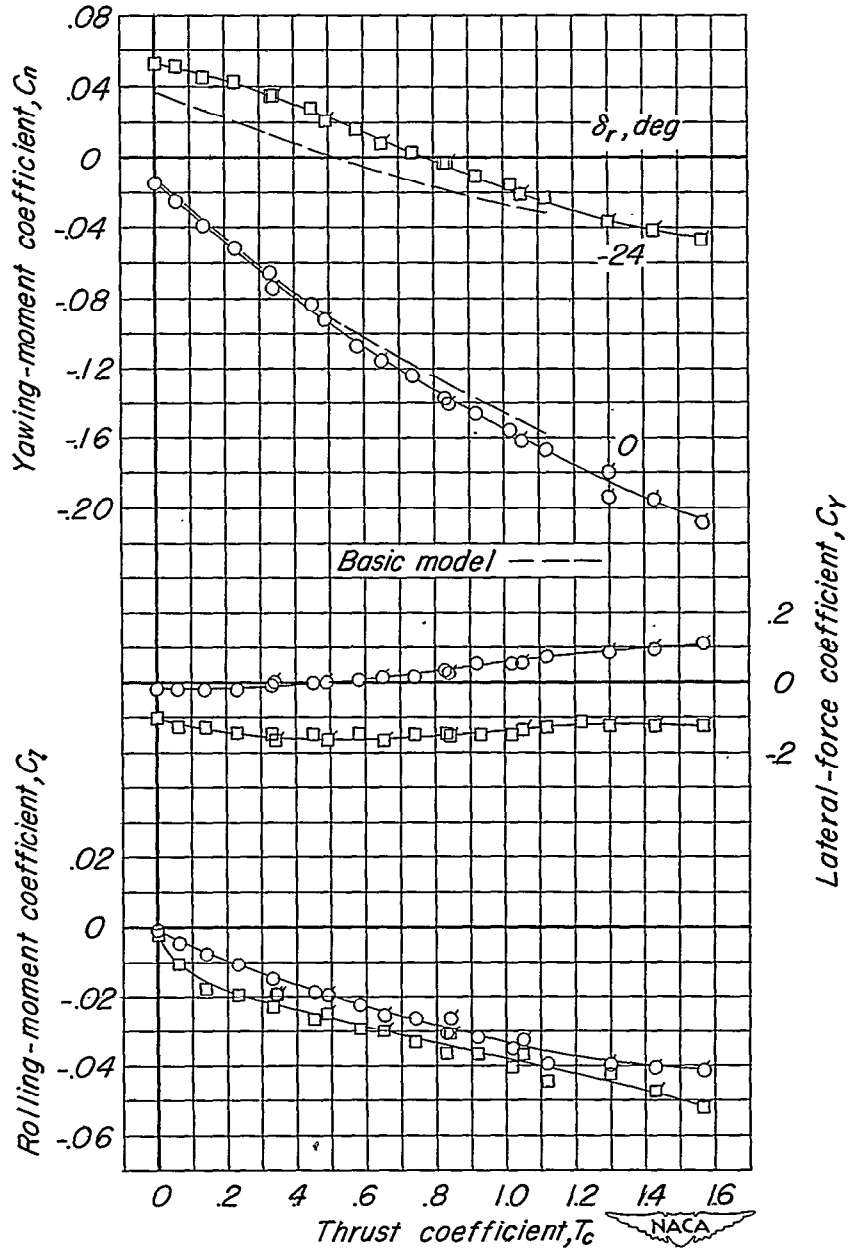
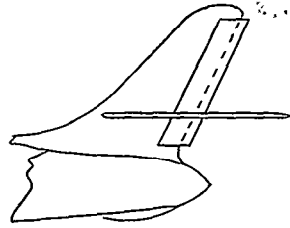
(c) Ventral fin.

(d) Dorsal fin. $\alpha = 11.4^\circ$.

Figure 14.- Continued.

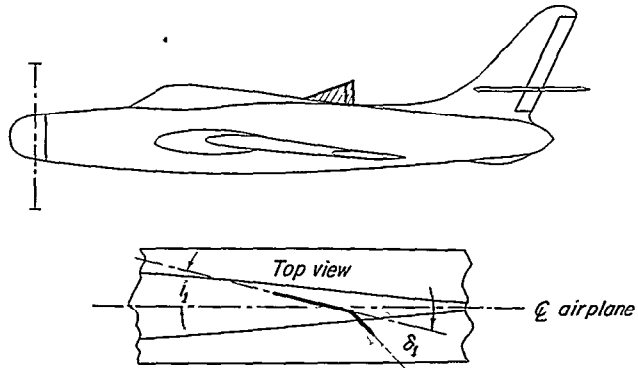


δ_r, deg
 ○ 0
 □ -24

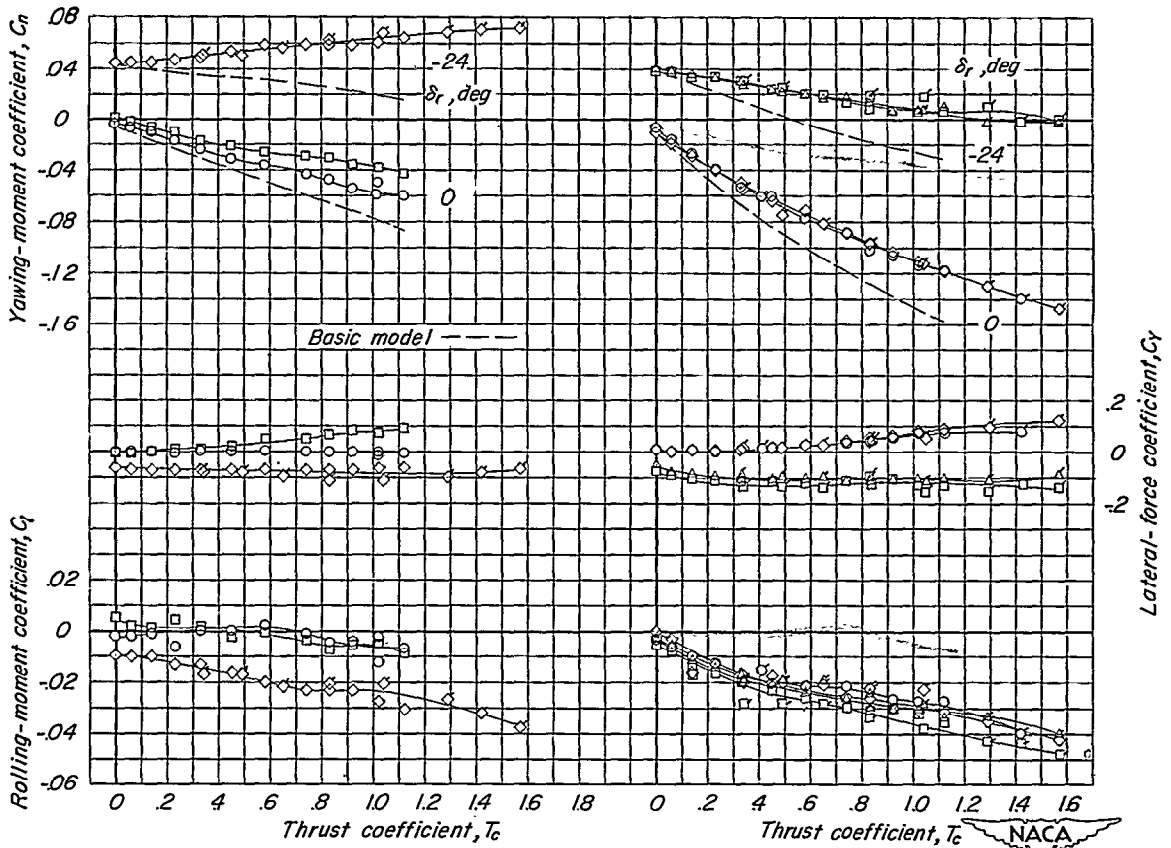


(e) Extended rudder chord. $\alpha = 11.4^\circ$.

Figure 14.- Concluded.



δ_r, deg	δ_t, deg	i_t, deg	δ_r, deg	δ_t, deg	i_t, deg
○	0	0	○	20	0
□	0	0	◇	0	10
◇	-24	0	□	-24	0
			△	-24	0



(a) $\alpha = 2.8^\circ$.

(b) $\alpha = 11.4^\circ$.

Figure 15.- Effect of a triangular dorsal fin on the directional trim characteristics. $\delta_f = 20^\circ$; $i_t = \delta_a = 0^\circ$; slats extended; $q = 6 \text{ lb/sq ft}$. (Flagged symbols indicate data at $q = 4 \text{ lb/sq ft}$.)

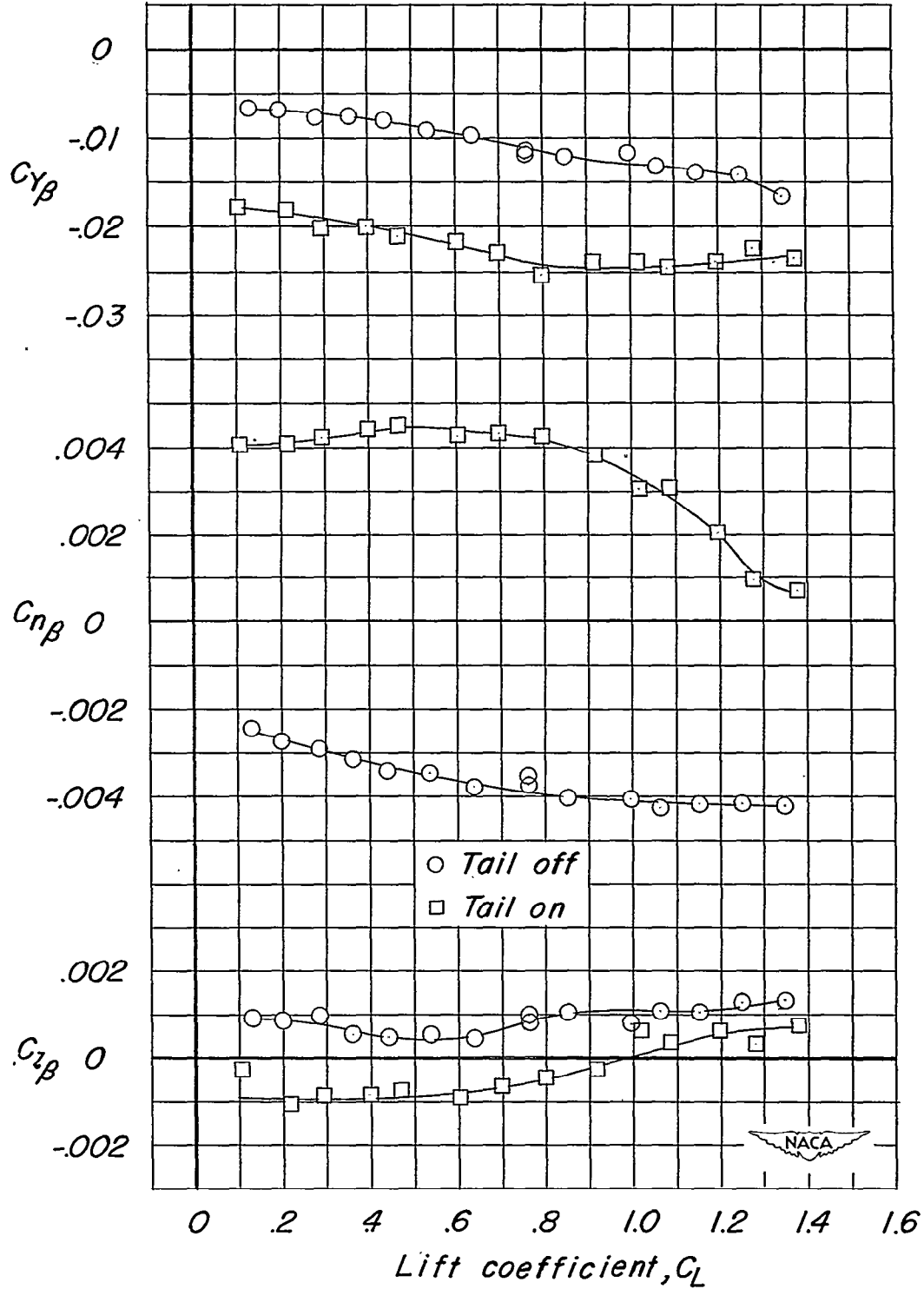
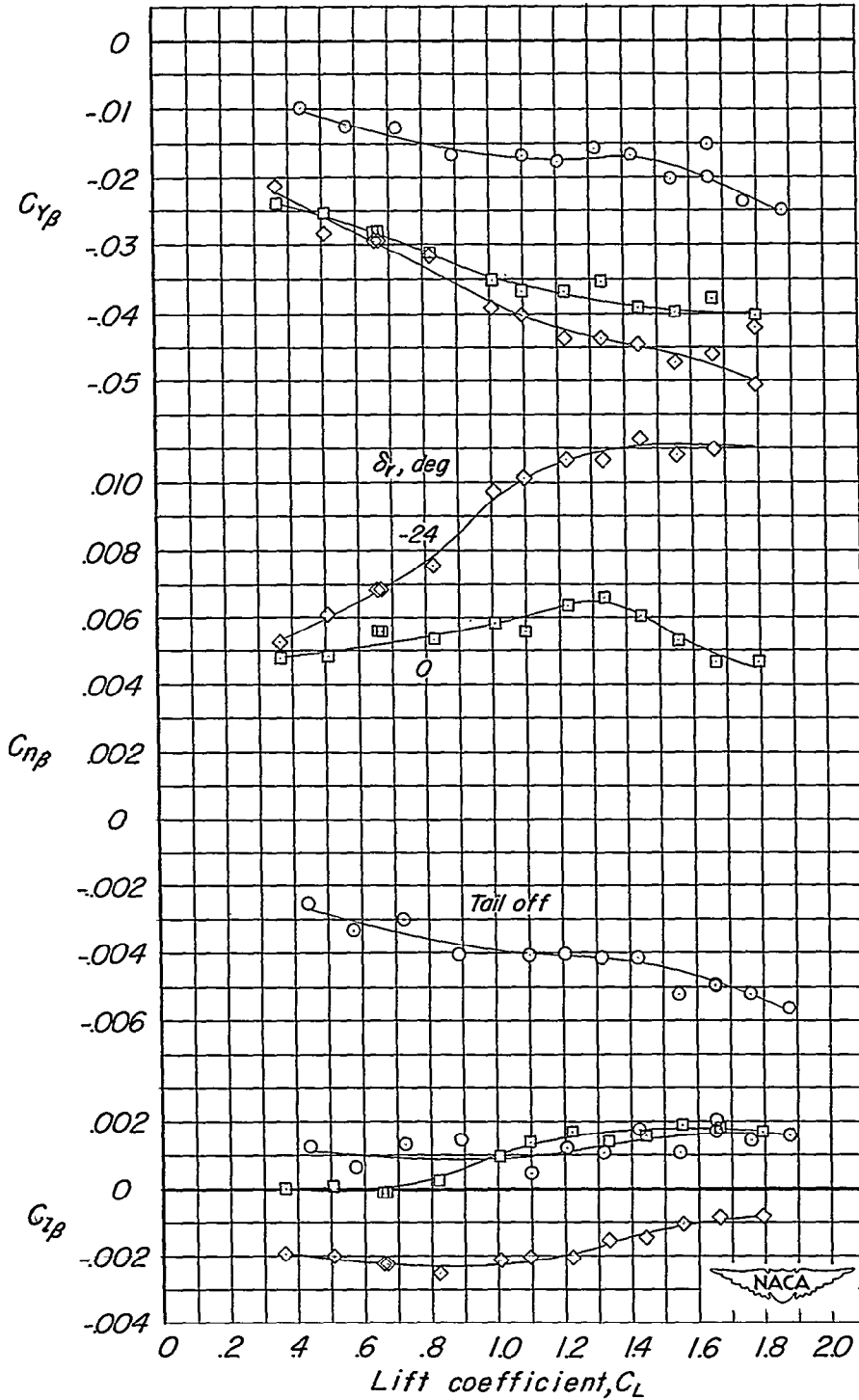
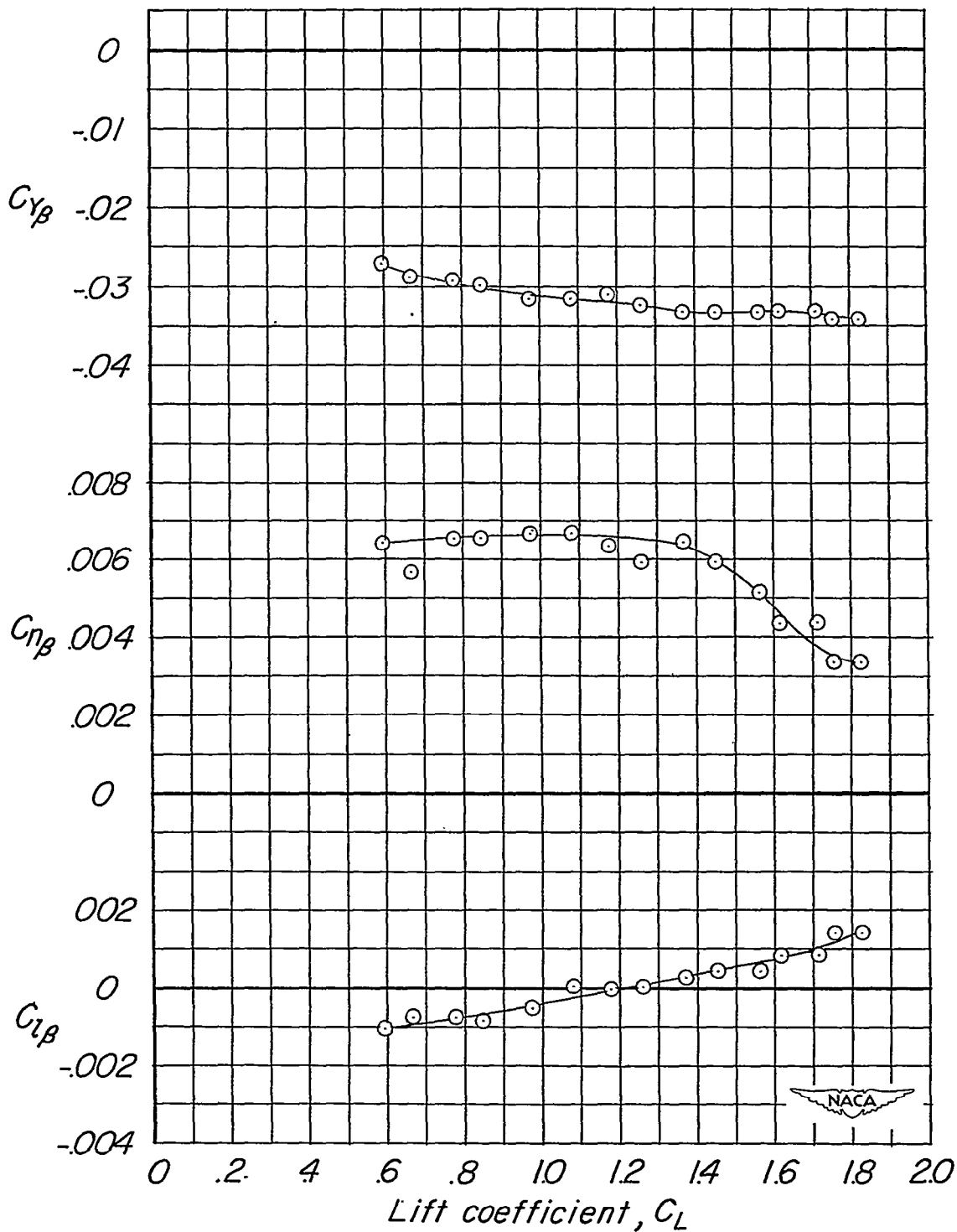
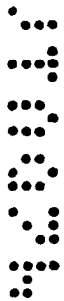


Figure 16.- Lateral-stability derivatives of the basic model with and without the horizontal and vertical tail. Power A; $\delta_f = \delta_a = \delta_r = 0^\circ$; $q = 8 \text{ lb/sq ft}$.



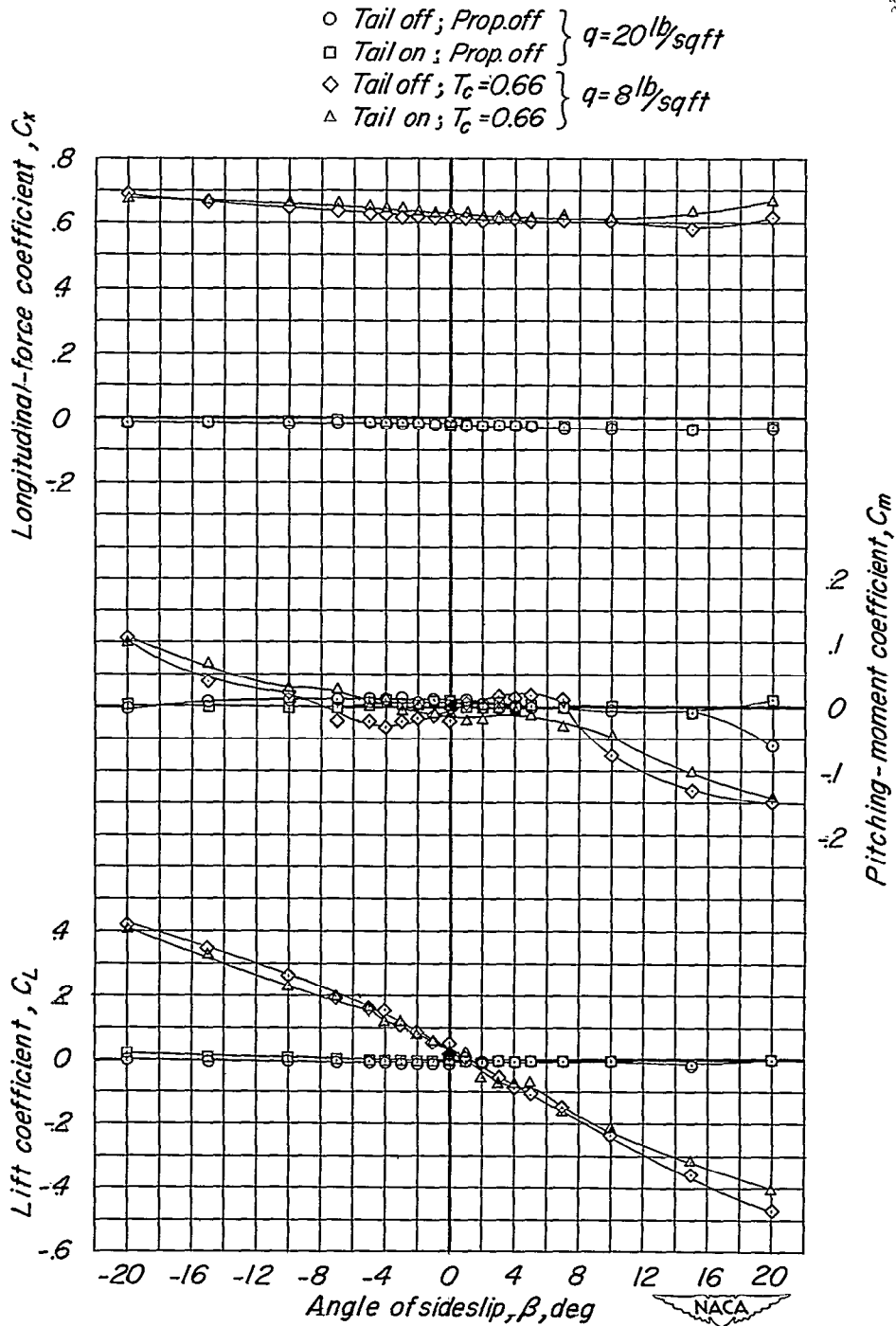
(a) Basic model. Power A; $q = 6$ lb/sq ft.

Figure 17.- Power-on lateral stability derivatives. $\delta_f = 40^\circ$; $\delta_a = 0^\circ$; slats extended.



(b) Complete model. Power B; $q = 8$ lb/sq ft.

Figure 17.- Concluded.

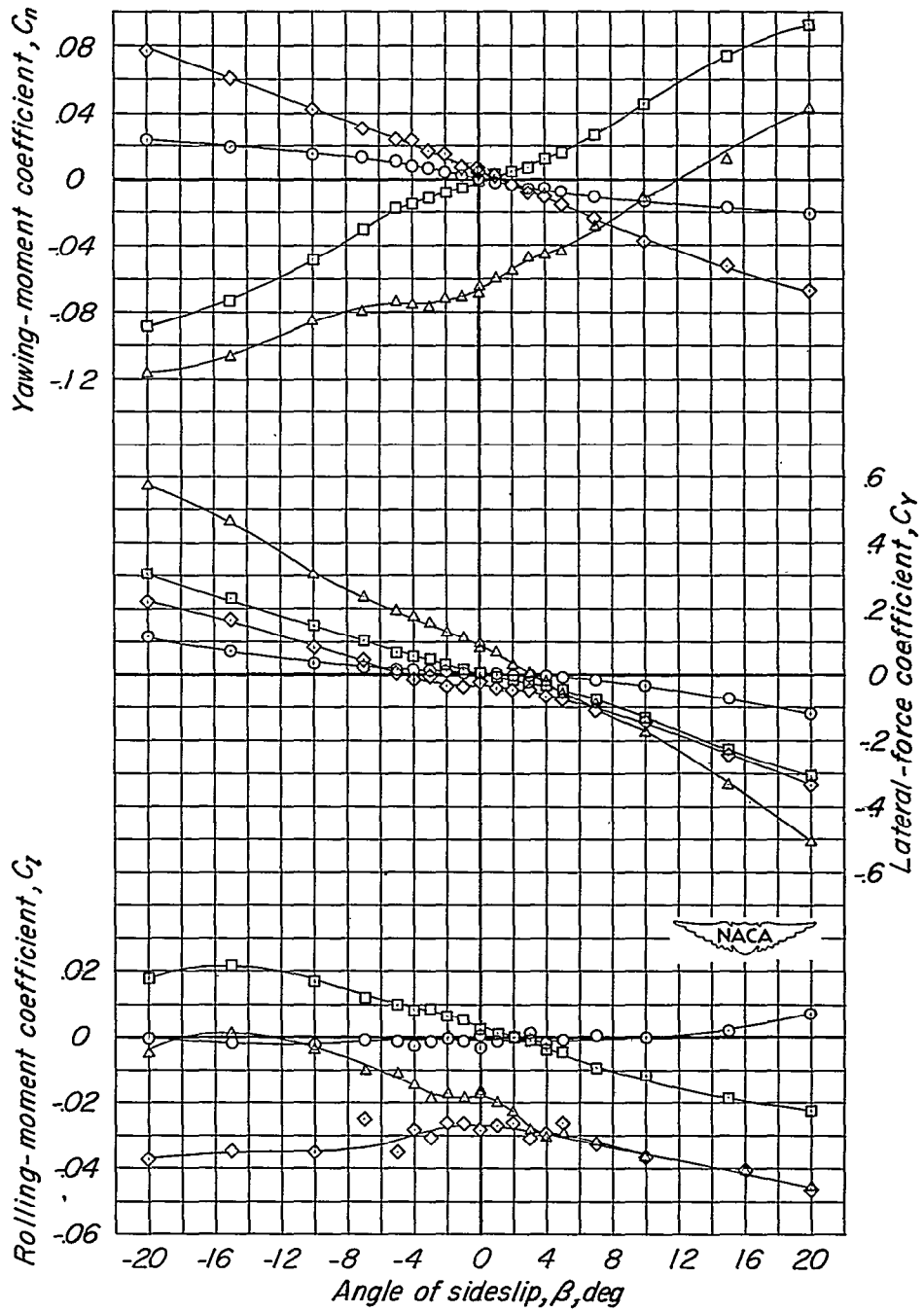


(a) Longitudinal characteristics.

Figure 18.- Aerodynamic characteristics in sideslip of the basic fuselage showing the effect of propeller operation and addition of the vertical tail. Wing, canopy, and protuberances removed from fuselage. $\alpha = 0^\circ$.

~~CONFIDENTIAL~~

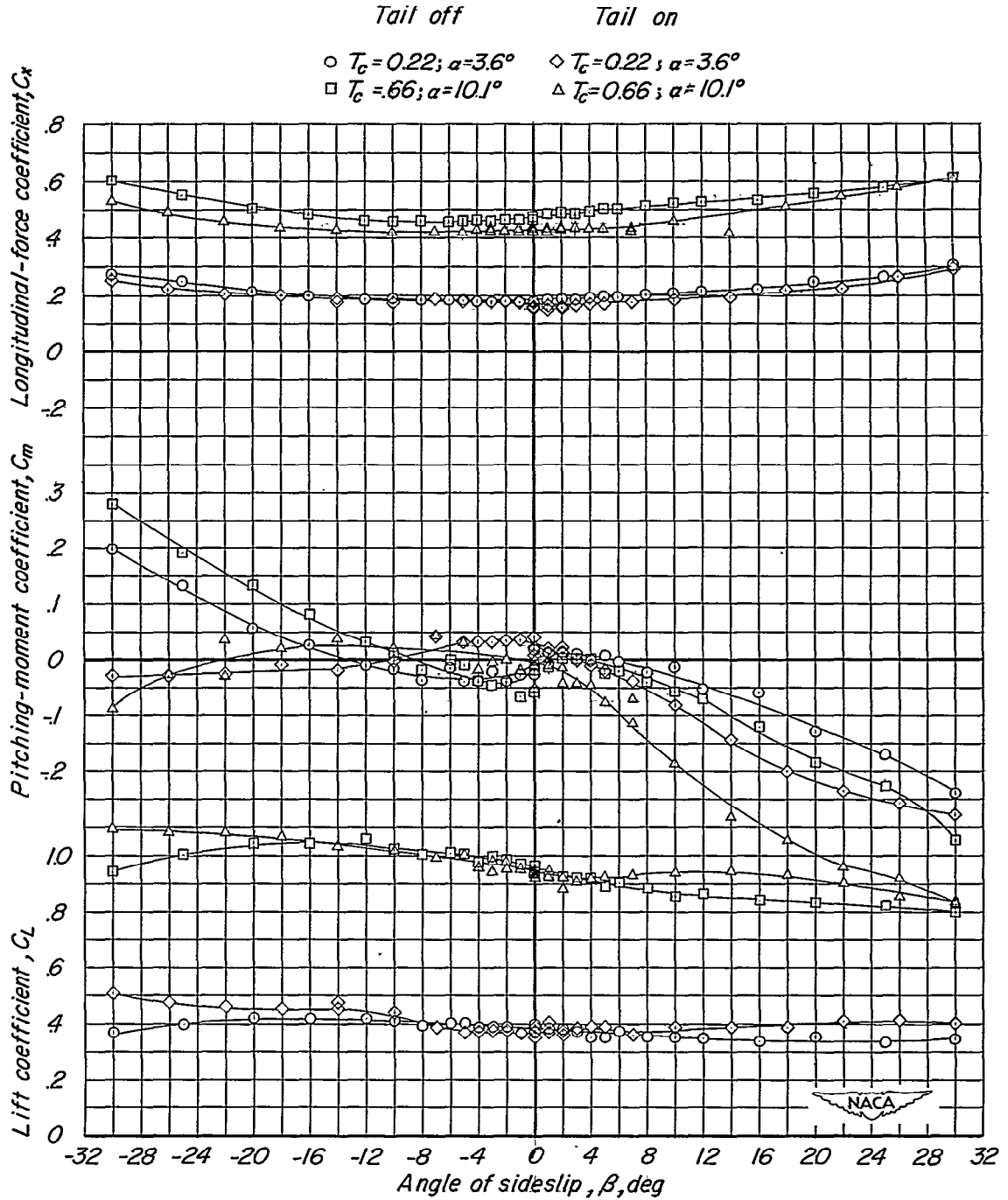
- Tail off; Prop. off } $q = 20 \text{ lb/sqft}$
- Tail on; Prop. off } $q = 20 \text{ lb/sqft}$
- ◇ Tail off; $T_c = 0.66$ } $q = 8 \text{ lb/sqft}$
- △ Tail on; $T_c = 0.66$ } $q = 8 \text{ lb/sqft}$



(b) Lateral characteristics.

Figure 18.- Concluded.

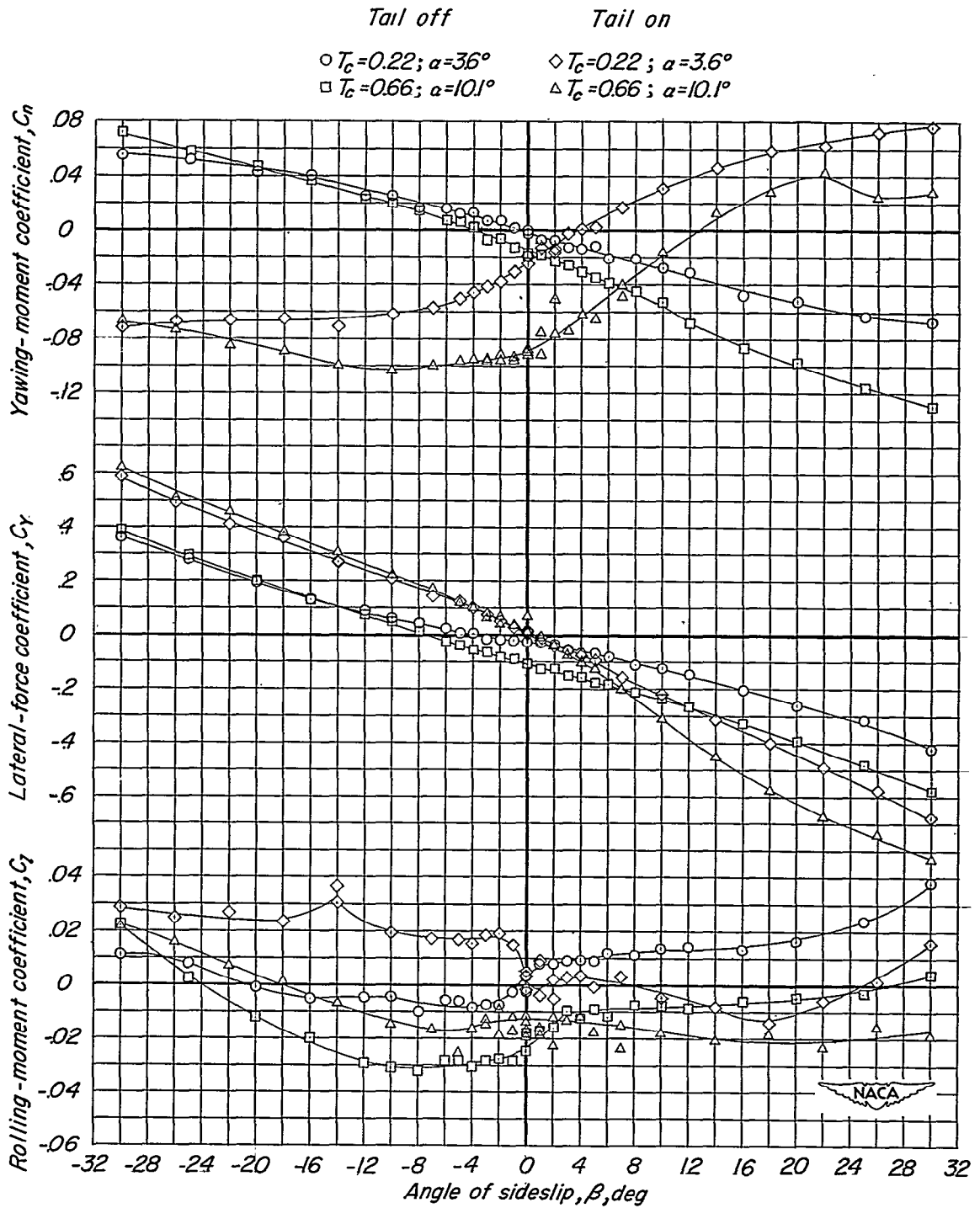
~~CONFIDENTIAL~~



(a) Longitudinal characteristics.

Figure 19.- Aerodynamic characteristics in sideslip of the basic model showing the effect of the horizontal and vertical tail surfaces for two constant-power thrust coefficients. $\delta_f = i_t = \delta_a = \delta_r = 0^\circ$; power A; $q = 8$ lb/sq ft.

~~CONFIDENTIAL~~

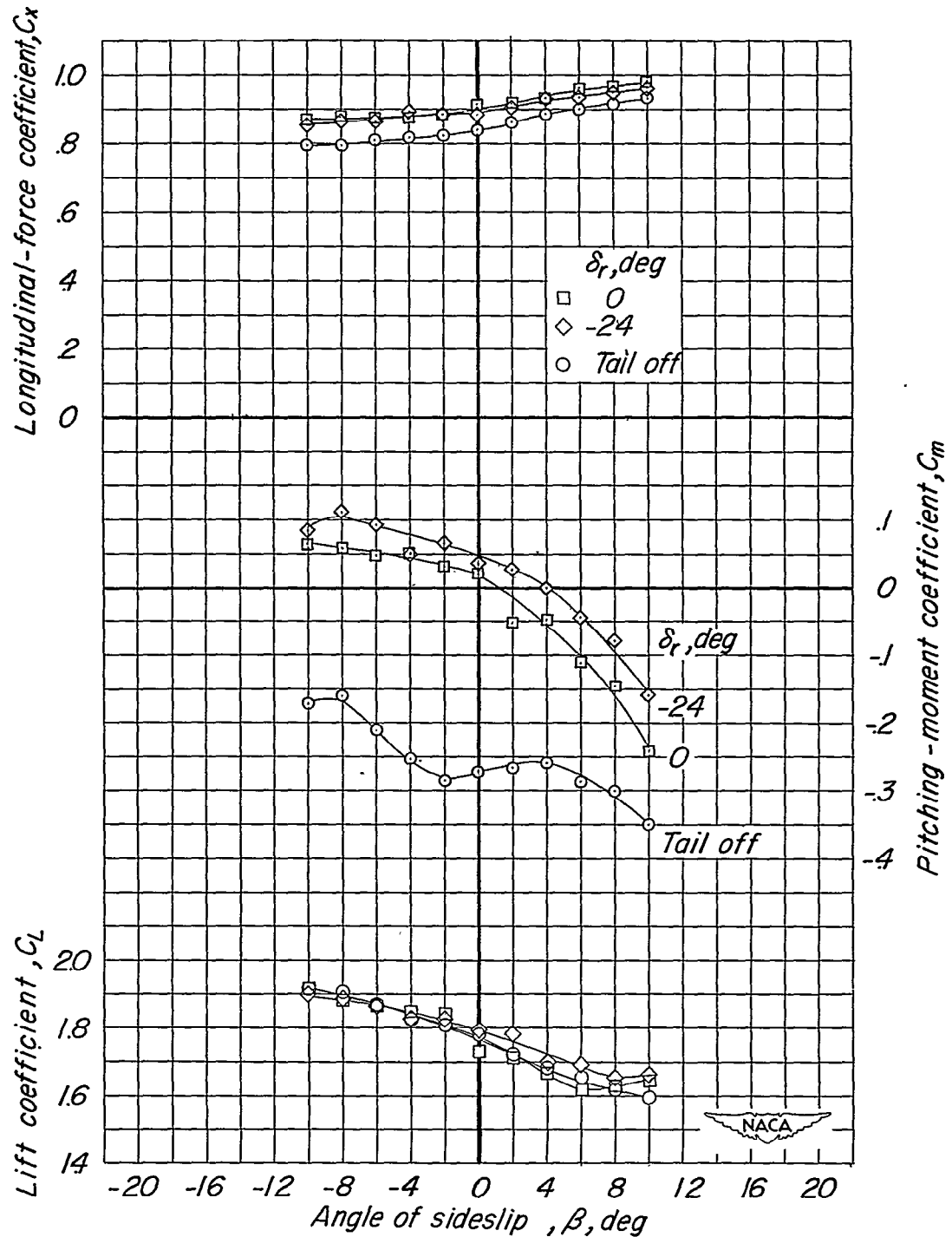


(b) Lateral characteristics.

Figure 19.- Concluded.

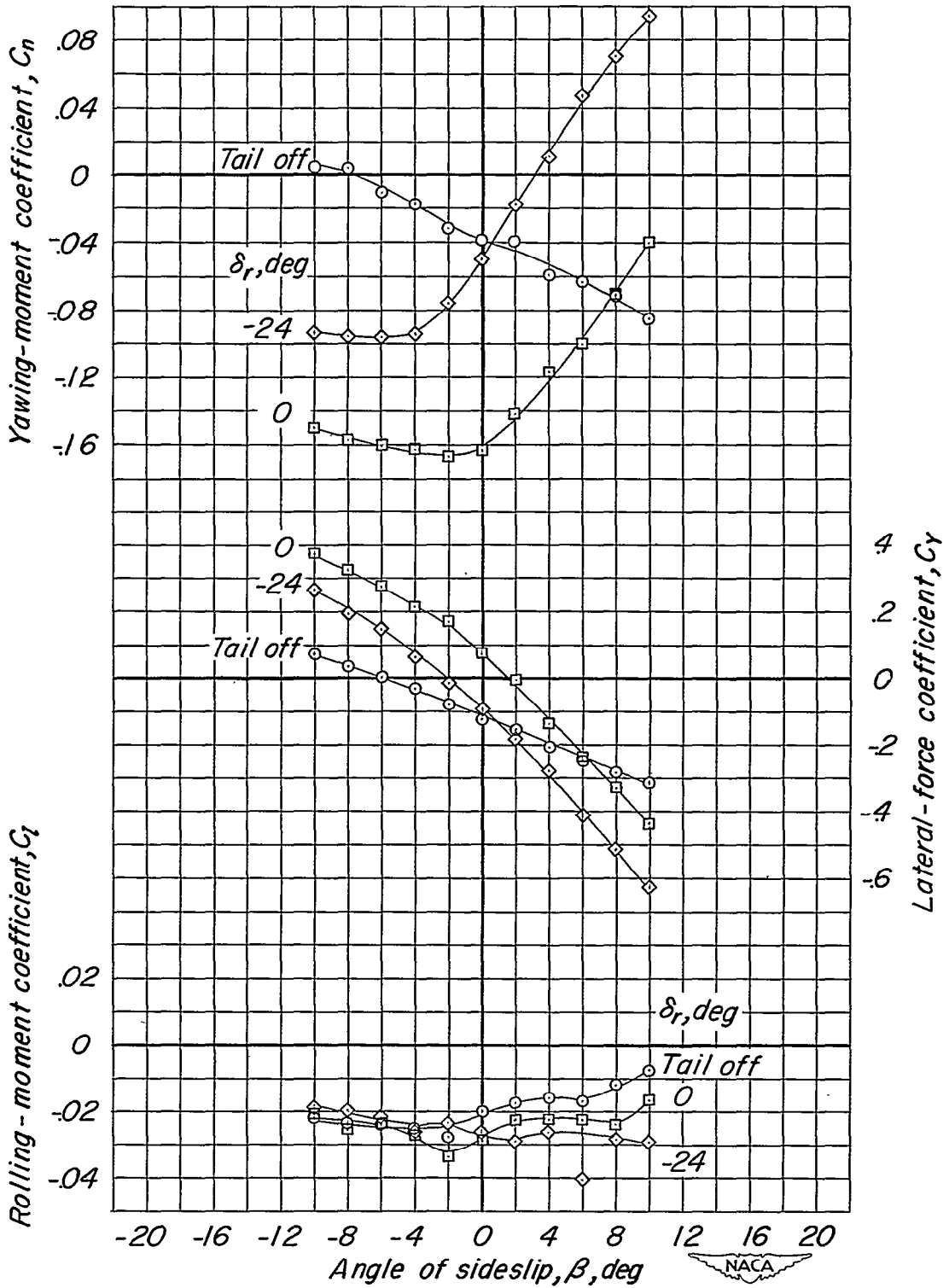
~~CONFIDENTIAL~~

20



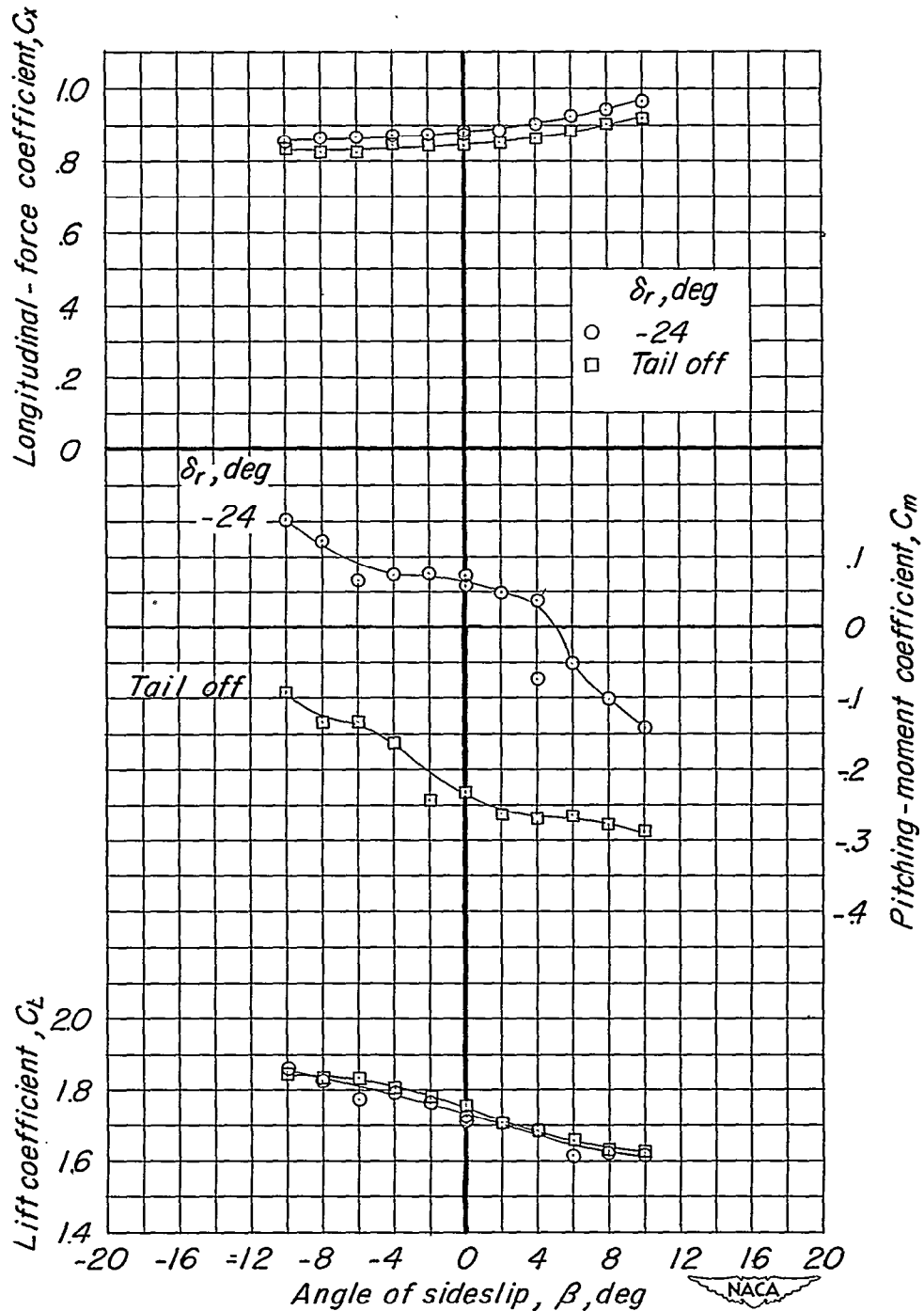
(a) Longitudinal characteristics.

Figure 20.- Aerodynamic characteristics in sideslip of the basic model showing effects of the tail surfaces and rudder deflection. $\delta_F = 40^\circ$; $i_t = -3^\circ$; $\delta_a = 0^\circ$; slats extended; $T_c = 1.45$; $\alpha = 10.4^\circ$; $q = 6$ lb/sq ft.



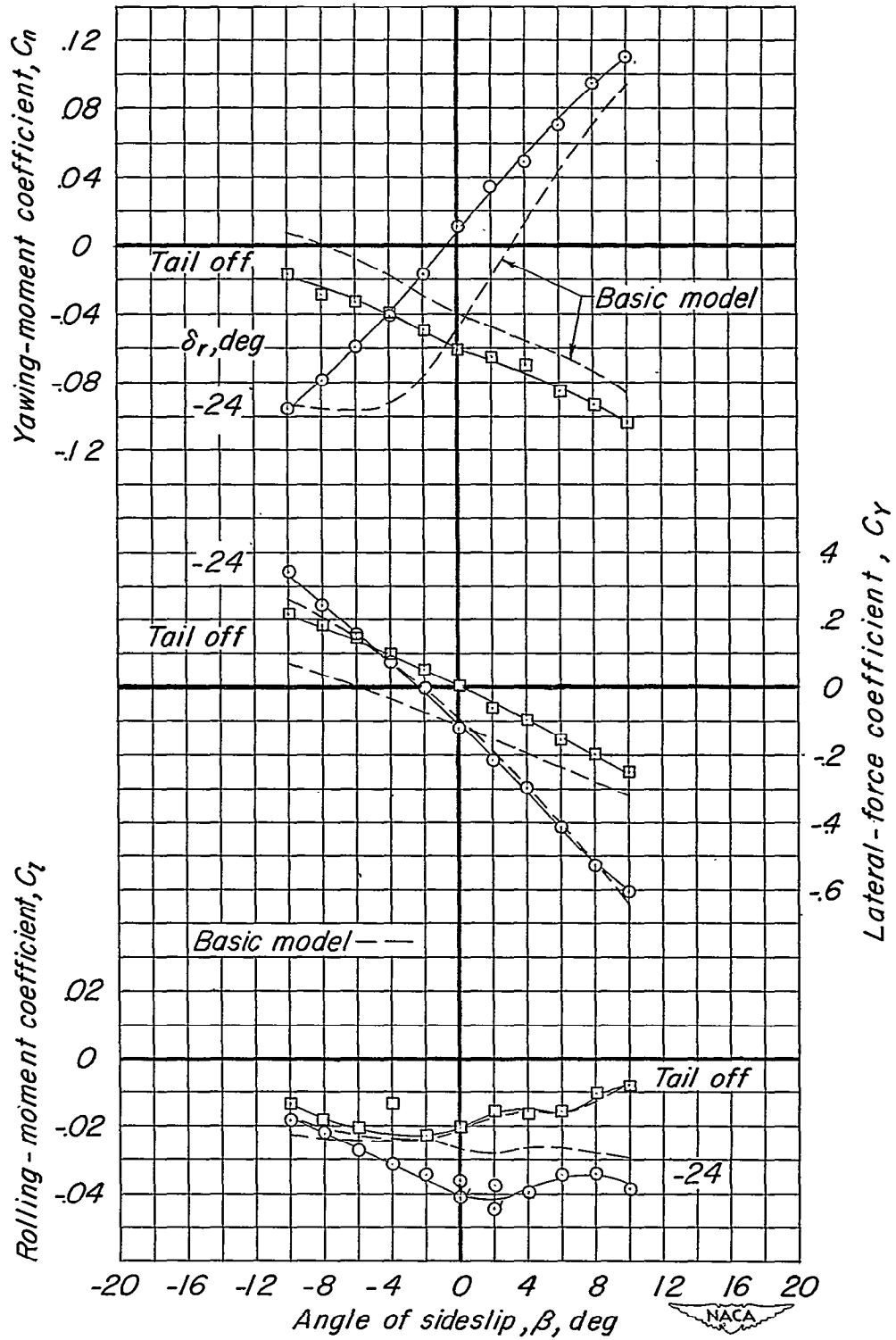
(b) Lateral characteristics.

Figure 20.- Concluded.



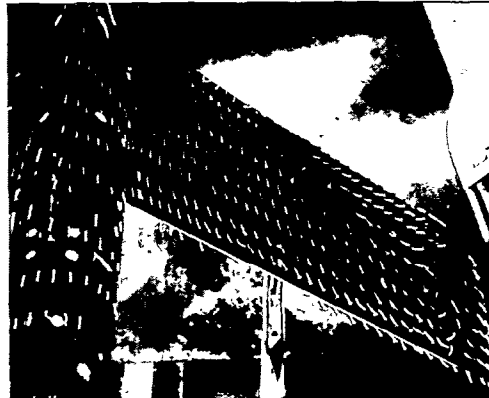
(a) Longitudinal characteristics.

Figure 21.- Aerodynamic characteristics in sideslip of the model with the triangular dorsal fin. $\delta_f = 40^\circ$; $i_t = 3^\circ$; $\delta_a = 0^\circ$; $\delta_l = 20^\circ$; $T_c = 1.45$; $\alpha = 10.2^\circ$; slats extended; $i_l = 0^\circ$; $q = 6$ lb/sq ft.

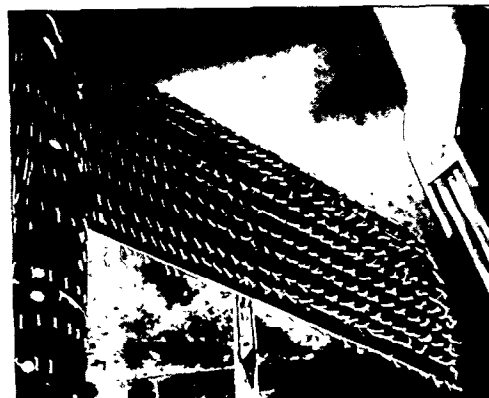
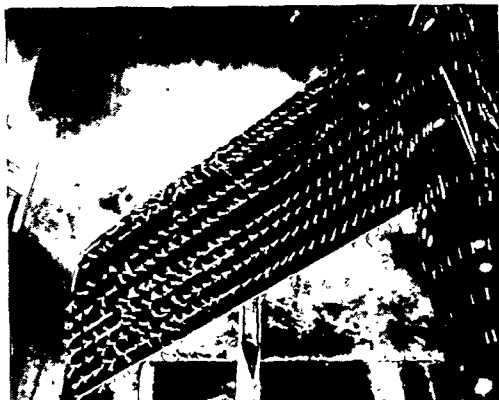


(b) Lateral characteristics.

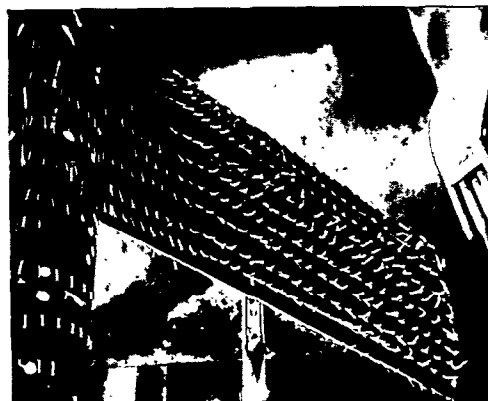
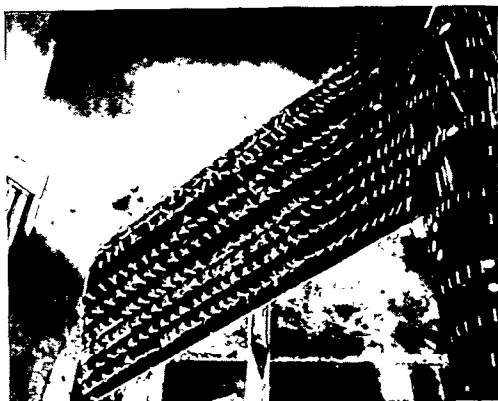
Figure 21.- Concluded.



$\alpha=6.7^\circ; C_L=0.55$



$\alpha=11.0^\circ; C_L=0.82$



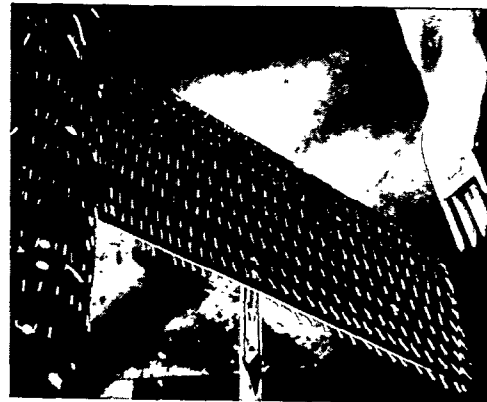
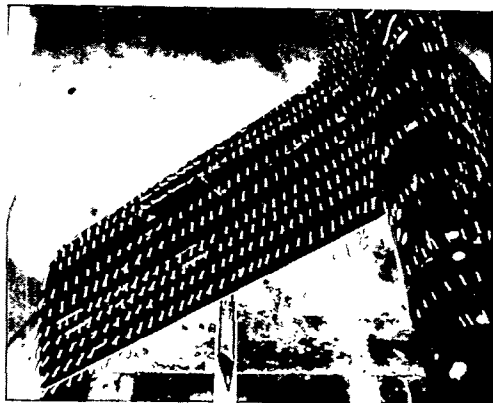
$\alpha=15.1^\circ; C_L=0.92$

L-80219

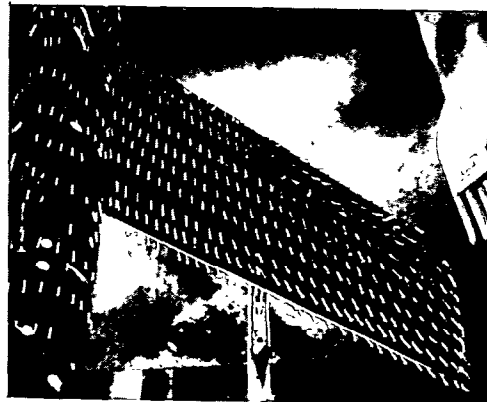
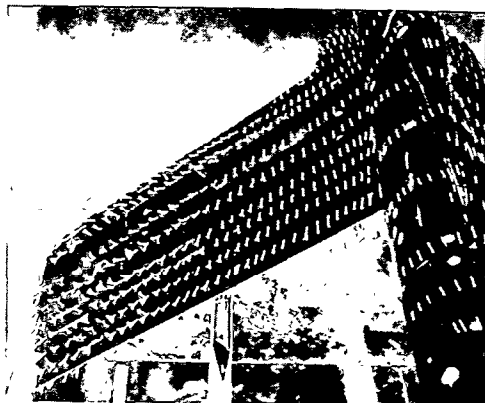
(a) Propeller windmilling. $\delta_f = 0^\circ$.

Figure 22.- Photographs of wing-surface tufts for the basic configuration.

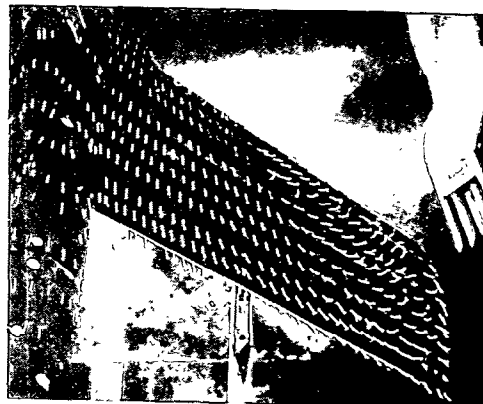
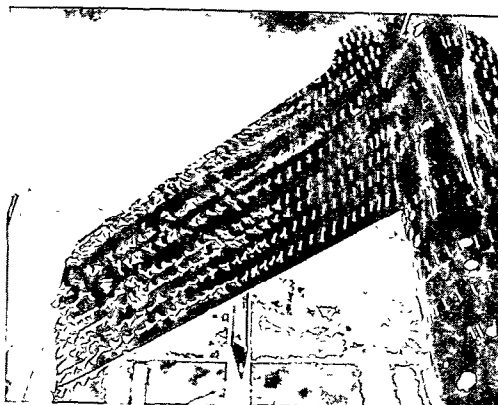
1
2
3
4
5
6
7
8
9
10
11
12
13
14
15
16
17
18
19
20
21
22
23
24
25
26
27
28
29
30
31
32
33
34
35
36
37
38
39
40
41
42
43
44
45
46
47
48
49
50
51
52
53
54
55
56
57
58
59
60
61
62
63
64
65
66
67
68
69
70
71
72
73
74
75
76
77
78
79
80
81
82
83
84
85
86
87
88
89
90
91
92
93
94
95
96
97
98
99
100



$\alpha = 4.7^\circ; C_L = 0.54$



$\alpha = 6.8^\circ; C_L = 0.71$



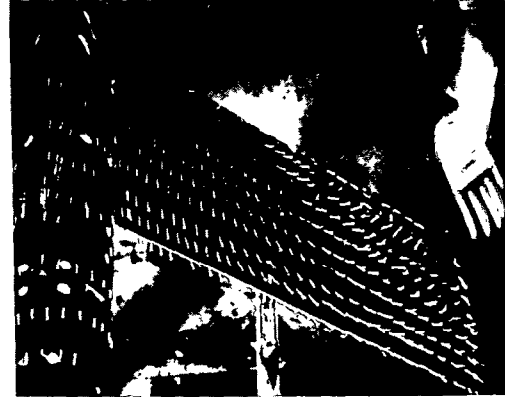
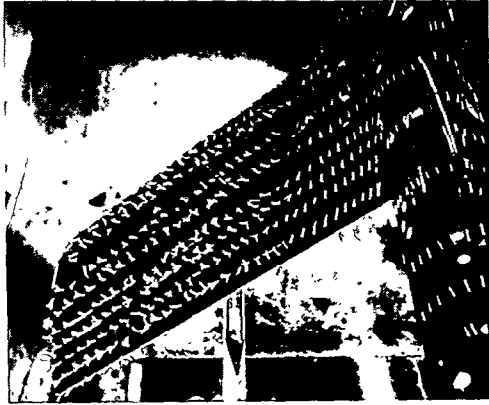
$\alpha = 9.0^\circ; C_L = 0.90$

L-80220

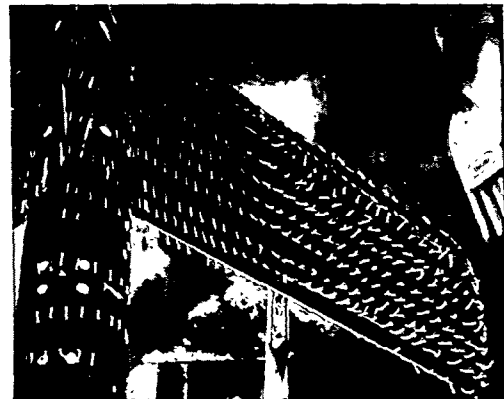
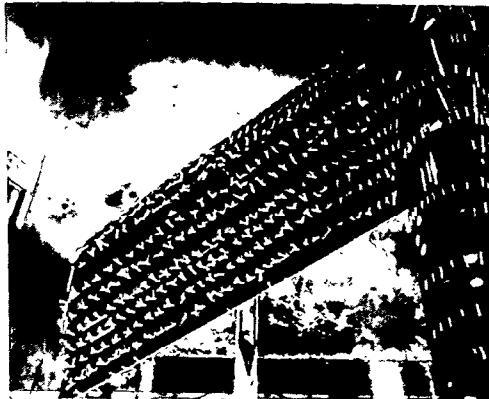
(b) $T_c = 0.66; \delta_F = 0^\circ$.

Figure 22.- Continued.

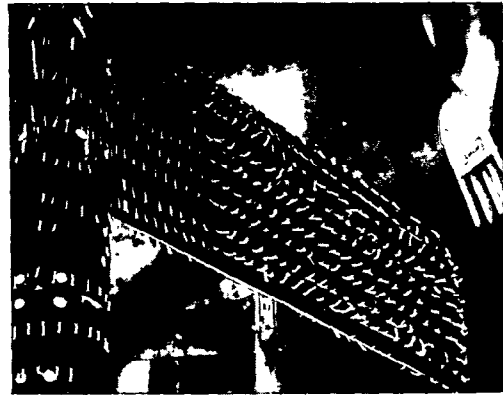
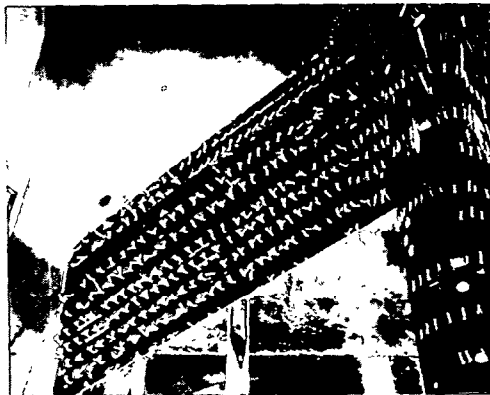
~~CONFIDENTIAL~~



$\alpha=11.1^\circ ; C_L=1.02$



$\alpha=15.2^\circ ; C_L=1.25$



$\alpha=19.4^\circ ; C_L=1.32$

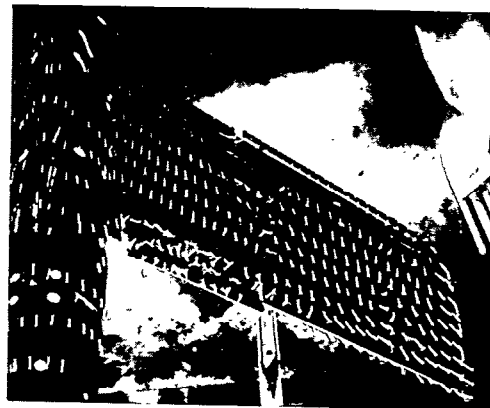
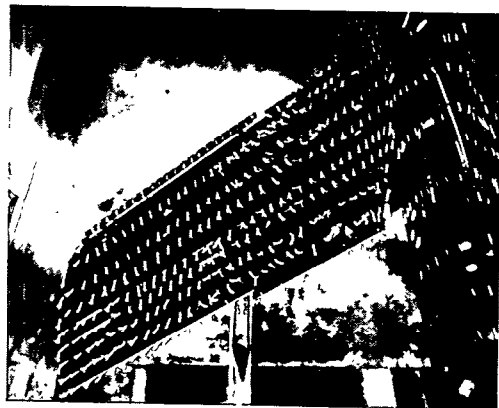
L-80221

(b) Concluded.

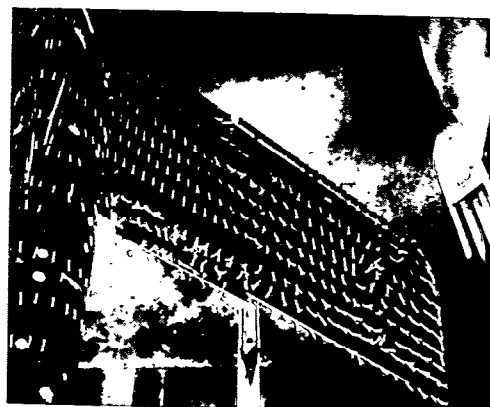
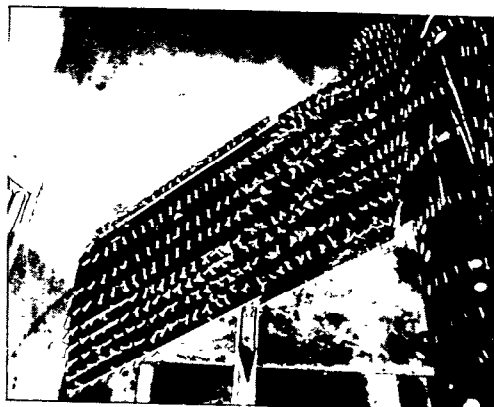
Figure 22.- Continued.

~~CONFIDENTIAL~~

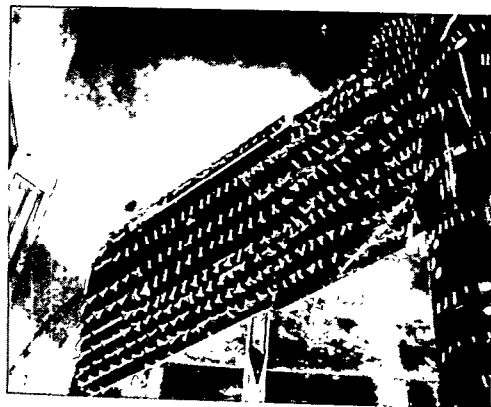
CONFIDENTIAL



$\alpha = 11.2^\circ$



$\alpha = 13.5^\circ$



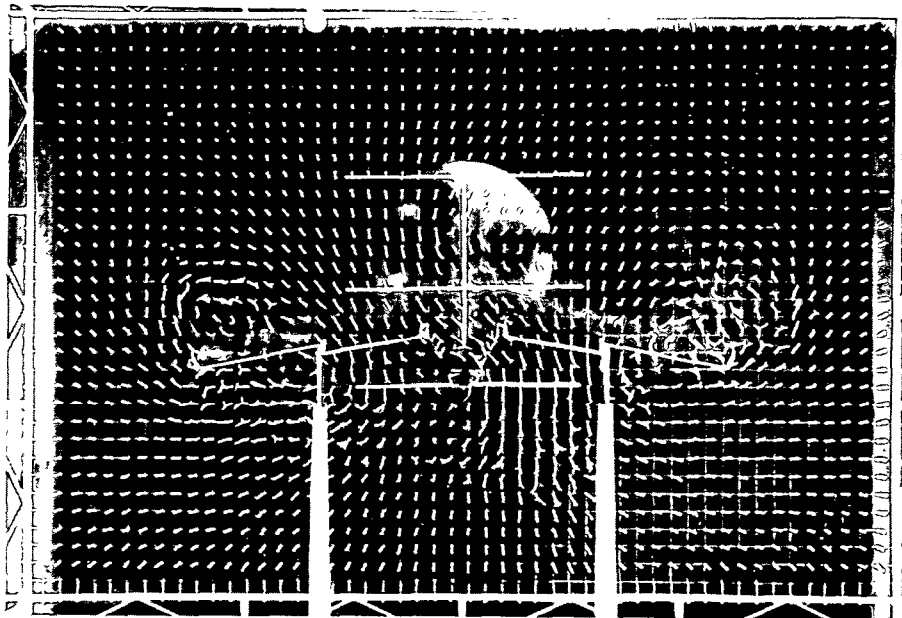
$\alpha = 17.5^\circ$

L-80222

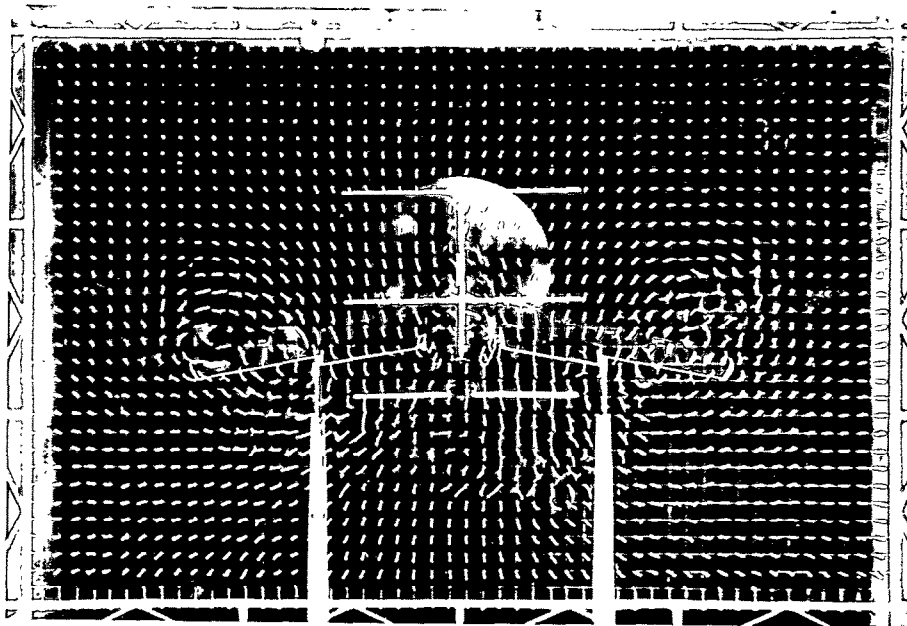
(c) Slats extended. $T_c = 0.96$; $\delta_f = 40^\circ$.

Figure 22.- Concluded.

CONFIDENTIAL



Basic configuration

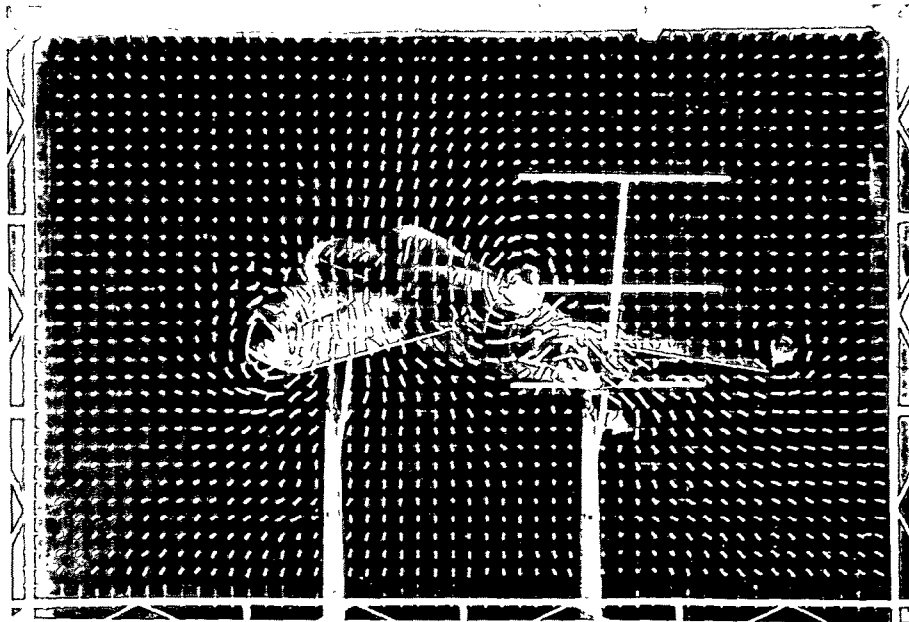


Triangular fin on ; $\delta_1 = 20^\circ$

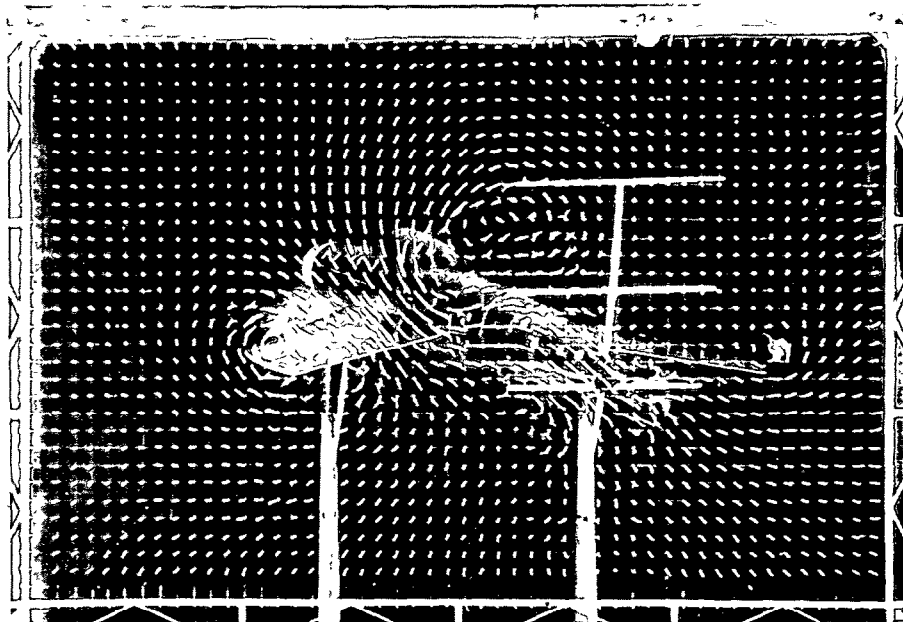
L-80223

(a) Effect of triangular fin. $T_c = 0.84$; $\delta_f = 20^\circ$; $\alpha = 11.4^\circ$.

Figure 23.- Tuft-grid photographs of flow field behind the model.



$\beta = 25^\circ$; Propeller windmilling

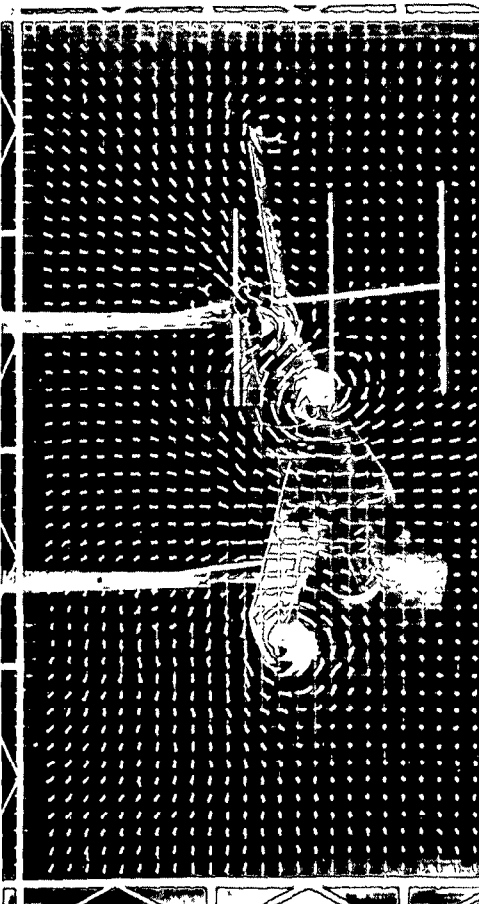


$\beta = 25^\circ$; $T_c = 0.66$

L-80224

(b) Effect of power with model in sideslip. $\delta_f = 0^\circ$; $\alpha = 10.3^\circ$.

Figure 23.- Continued.



$\beta = -25^\circ$; Propeller windmilling



$\beta = -25^\circ$; $T_c = 0.66$

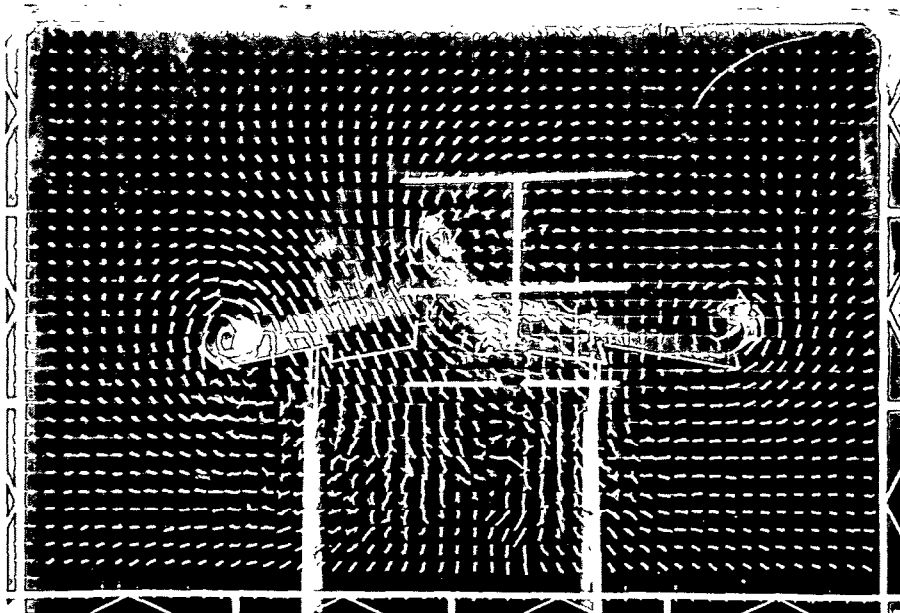
L-80225

(b) Concluded.

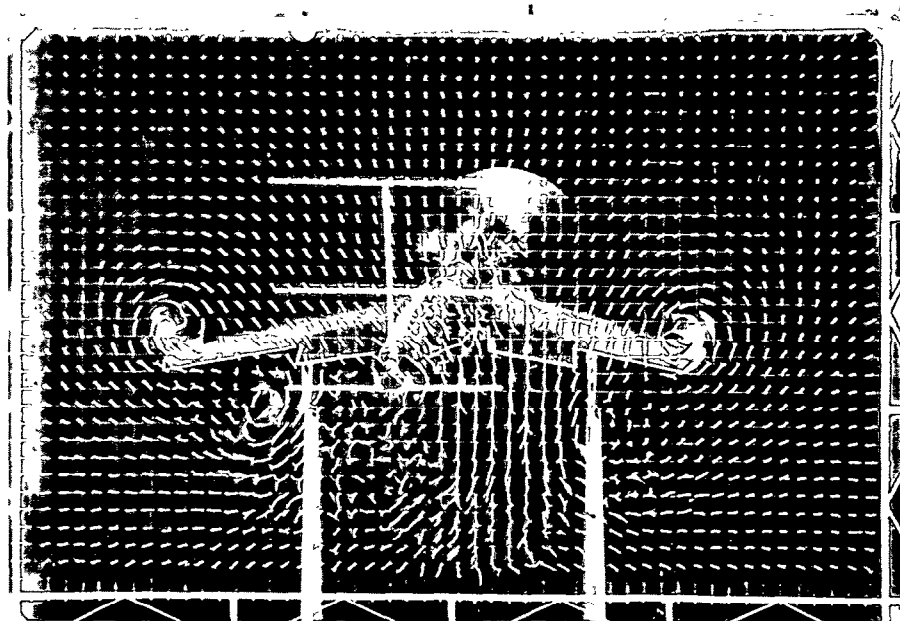
Figure 25.- Continued.

A small horizontal line with a vertical tick mark at the right end, likely a scale or reference marker.

CONFIDENTIAL



$\beta = 10^\circ ; T_c = 1.45$



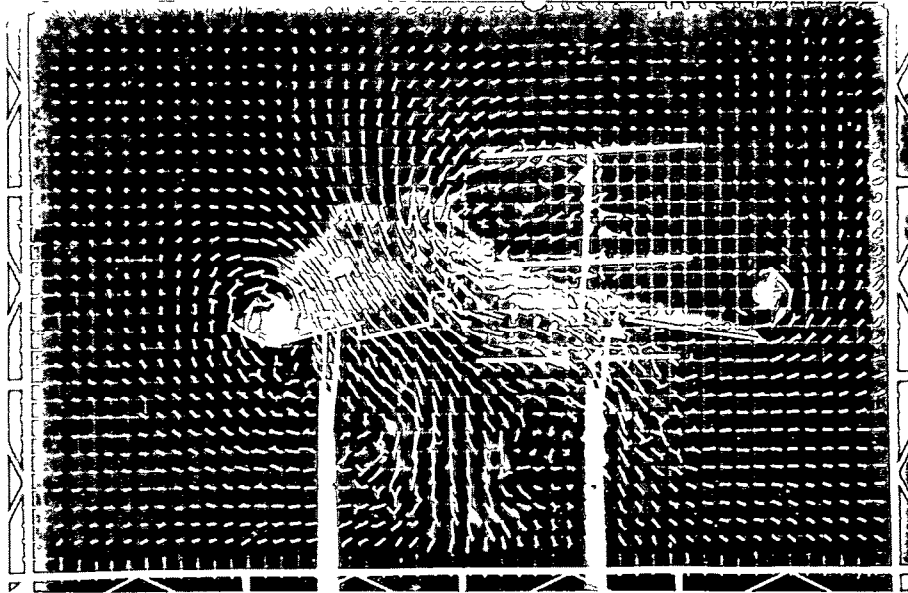
$\beta = -10^\circ ; T_c = 1.45$

L-80226

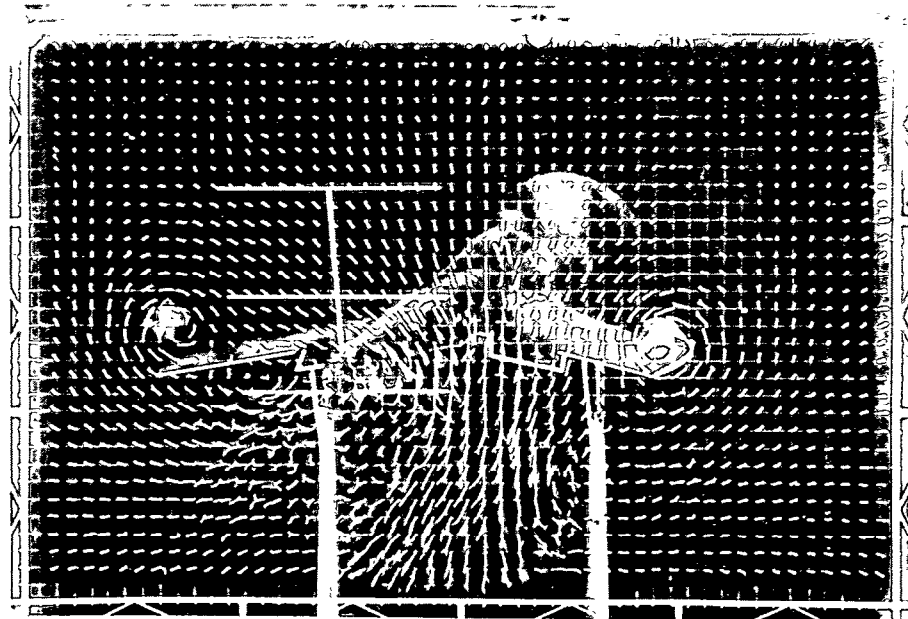
(c) Effect of sideslip. $\delta_f = 40^\circ ; T_c = 1.45 ; \alpha = 10.4^\circ$.

Figure 23.- Continued.

1
2
3
4
5
6
7
8
9
10
11
12
13
14
15
16
17
18
19
20
21
22
23
24
25
26
27
28
29
30
31
32
33
34
35
36
37
38
39
40
41
42
43
44
45
46
47
48
49
50
51
52
53
54
55
56
57
58
59
60
61
62
63
64
65
66
67
68
69
70
71
72
73
74
75
76
77
78
79
80
81
82
83
84
85
86
87
88
89
90
91
92
93
94
95
96
97
98
99
100



$\beta = 20^\circ; T_c = 1.45$



$\beta = -20^\circ; T_c = 1.45$

L-80227

(c) Concluded.

Figure 23.- Concluded.

~~CONFIDENTIAL~~

SECURITY INFORMATION

NASA Technical Library



3 1176 01438 6040

[REDACTED]